Ruben Felipe Oblitas Torrico

Preparação e caracterização de híbridos orgânico-inorgânicos à base de epoxí-silica

Dissertação apresentada ao Instituto de Química da Universidade Estadual Paulista "Júlio de Mesquita Filho" Campus de Araraquara, para obtenção Titulo de Mestre em Química (área de concentração : Físico-química

Orientador : Prof. Dr. Peter Hammer

Araraquara
2016

FICHA CATALOGRÁFICA

Oblitas Torrico, Ruben Felipe Arturo
O12p Preparação e caracterização de híbridos orgânico-inorgânicos a base de epóxi-sílica / Ruben Felipe Arturo Oblitas Torrico. – Araraquara: [s.n.], 2016
68 f.: il.

Dissertação (mestrado) – Universidade Estadual Paulista, Instituto de Química
Orientador: Peter Hammer

1. Híbridos orgânico-inorgânicos. 2. Processo sol-gel. 3. Dispositivos de filme fino.4. Resinas epóxi. 5. Eletroquímica. I. Título

Elaboração: Seção Técnica de Aquisição e Tratamento da Informação

Biblioteca do Instituto de Química, Unesp, câmpus de Araraquara

RUBEN FELIPE ARTURO OBLITAS TORRICO

Dissertação apresentada ao Instituto de Química, Universidade Estadual Paulista, como parte dos requisitos para obtenção do título de Mestre em Química.

Araraquara, 15 de abril de 2016.

BANCA EXAMINADORA

Prof. Dr. Peter Hammer (Orientador)
Instituto de Química – UNESP, Araraquara

Prof. Dr. Cecilio Sadao Fugivara
Instituto de Química – UNESP, Araraquara

Prof. Dr. Hudson Wallace Pereira de Carvalho
Centro de Energia Nuclear na Agricultura – USP, Piracicaba

DADOS CURRICULARES

1. DADOS PESSOAIS

Nome: Ruben Felipe Arturo Oblitas Torrico
Endereço Profissional: Av. Prof. Francisco Degni, 55 - Jardim Quitandinha, Araraquara –SP
E-mail: ro1485@my.bristol.ac.uk

2. FORMACAO ACADEMICA

2.1

Bacharelado em ciências, Université de Montpellier, Montpellier-Franca, concluído em 2012

2.2

Bacharelado em Físico Química, University of Bristol, Bristol-UK, não concluído

3. PRODUÇÃO CIENTIFICA

3.1 Participação em eventos científicos

- Workshop em Computational Chemistry for Interacting system , School of Chemistry and Centre for Computational Chemistry University of Bristol, UK, 2012
- Escola de inverno, Ótica moderna e Fotonica, Universidade Estadual de Campinas,Campinas Brasil,2014
- Impacto da Cristalografia nas Diferentes Áreas da Ciência, Instituto de Química, Unesp, Araraquara, Brasil,2014
- Escola SAXS e SANS, Universidade católica de Rio de Janeiro, PUC, Rio de Janeiro, Brasil, 2015

AGRADECIMENTO

Ao Brasil pela acolhida

A minha Mae

A minha Família

Ao meu orientador Peter Hammer, pelo apoio

A todos os membros do Grupo de Físico-química de Materiais. Agradeço especialmente a Ranielle Oliveira da Silva pela amizade

A todas as pessoas que conheci em Araraquara

Aos órgãos de fomento

RESUMO

Este projeto visa a investigar a relação entre a estrutura e as propriedades dos materiais epoxi-silica preparados pelo método sol-gel. Os híbridos foram preparados pela reação de cura entre o poly(Bisphenol A-co-epichlorohydrin) (DGBEA) , e o dietil triamina (DETA) assim como pelo processo Sol-Gel de hidrolise e condensação entre GPTMS (3-Glycidoxypropyl)methyldiethoxysilane) e TEOS. Ressonância magnética nuclear (RMN), espectroscopia de fotoelétrons de raios X (XPS), espalhamento de raios X a baixo ângulo (SAXS), espectroscopia de Infravermelho e RAMAN, microscopia de força atômica (AFM) assim como termogravimétria foram utilizadas com o proposito de investigar a morfologia e as propriedades estruturais do material. Finalmente as propriedades anticorrosivas dos filmes foram testadas em uma solução salina por meio de espectroscopia de impedância eletroquímica (EIS). Durante a fase inicial do projeto diferentes amostras com diferentes concentrações de TEOS foram preparadas. A estabilidade térmica como as propriedades anticorrosivas foram testadas. Os resultados mostraram que para maiores concentrações de TEOS, as propriedades anticorrosivas e térmicas dos híbridos melhoram significativamente. Vários resultados interessantes foram obtidos, para híbridos com razoes molares de TEOS : GPTMS : DGBEA = 1 : 1: 1, tendo módulos de impedância de até 10^{10} Ω cm^{-2}. Durante a segunda fase do projeto, duas series de amostras com concentrações diferentes de GPTMS a TEOS foram preparadas. As propriedades estruturais foram obtidas por meio de Espectroscopia Infravermelho, Raman, RMN e XPS e espalhamento de raios X a baixo ângulo. A hidrofobicidade assim como as propriedades térmicas foram avaliadas por meio de testes de molhabilidade e análise termogravimétrica. Finalmente as propriedades anticorrosivas dos filmes em contato com solução salina foram testadas por meio de espectroscopia de impedância electroquímica.

ABSTRACT

This work aims to investigate the relationship between the structure and the properties of the sol-gel prepared epoxy-silica materials. The organic-inorganic hybrids were prepared from the curing reaction of poly(Bisphenol A-co-epichlorohydrin) (DGBEA), with Diethyltriamine (DETA) and (3-Glycidoxypropyl)methyltriethoxysilane) (GPTMS) combined with the sol-gel hydrolysis and condensation reactions between Tetraethoxysilane (TEOS) and GPTMS. Nuclear magnetic resonance (NMR), X-ray photoelectron spectroscopy (XPS), Infrared and Raman spectroscopy (IR), Atomic force microscopy, as well as thermogravimetry (TG) have been used with the purpose to investigate the morphological and structural properties of the material. Finally the anticorrosive properties of the hybrid coated carbon steel were evaluated in saline solution using electrochemical impedance spectroscopy (EIS). During the initial phase of the project different samples with increasing concentrations of TEOS have been prepared and their thermal stability as well as their anticorrosive properties were tested. It was found, that for increasing TEOS concentration, the hybrid's anticorrosive and thermal properties can be improved. Several interesting results were obtained for hybrid coatings at a TEOS : GPTMS : DGBEA = 1 : 1 : 1 ratio, having an impedance modulus of up to $10^{10}\ \Omega\ cm^{-2}$. During the second phase of the work, a series of epoxy-silica hybrids were synthetized varying the concentrations of GPTMS and TEOS. Their structural properties were characterized by means of Infrared, Raman, solid NMR and XPS spectroscopy. Their hydrophobicity as well as their thermal resistance were evaluated using the drop shape analysis and thermogravimetry. Finally the anticorrosive properties of the coatings in saline solution were tested using electrochemical impedance spectroscopy.

LIST OF FIGURES **Page**

LIST OF TABLES **Page**

LIST OF ABREVIATIONS

AFM	Atomic Force Microscopy
At %	Atomic percentage
C_d	Polycondensation degree
Cl^-	Chloride
cm	Centimeters
C_r	Chromium
DETA	Diethyltriamine
DGBEA	Poly(Bisphenol A-co-epichlorohydrin)
DTG	First derivative in the TG curve
Erf	Error function
EIS	Electrochemical Impedance Spectroscopy
E_{oc}	Open circuit potential
eV	Electron Volts
g	grams
GPTMS	(3-Glycidoxypropyl)trimethoxysilane
H_2O	Water
Hz	Hertz
IR	Infrared Spectroscopy
L	Liters
min	minutes
N_2	Nitrogen
NaCl	Sodium Chloride
Na	Sodium
nm	nanometers
NMR	Nuclear Magnetic Resonance
O_2	Oxygen
ppm	Parts per Millon
R_g	Radius of Gyration
RMS	Root Mean Square
R_{rms}	RMS roughness
SAXS	Small Angle Scattering
SEM	Secondary Electron Microscopy

Si	Silicon
SiO_2	Silica
TEOS	Tetra ethoxy silane
TG	Thermogravimetry
THF	Tetrahydrofurane
Arb.u.	Arbitrary units
XPS	X-ray photoelectron spectroscopy
wt%	Mass percentage
Z	Impedance
μF	Micro faraday
μm	Micrometers
Ω	Ohm
Θ	Contact angle
°C	Celcius Degrees

CONTENTS

1 INTRODUCTION

One of today's great industrial challenges is the reduction of costs resulting from the corrosion of metallic materials. This natural phenomenon transforming metals in their natural ore causes huge losses and a lot of effort is put to limit its impact. One way to protect metallic materials from corrosion is by the reduction of Cr^{6+} to Cr^{3+}, this process known as passivation forms a stable layer of chromium oxide that prevents the diffusion of corrosive species. However one of the big problems comes from the hexavalent chromium is that is highly toxic. Therefore, alternatives are needed for efficient and environmental compliant coatings. In this context thin-films based on epoxy resins are an interesting candidate. However pure organic coatings have several disadvantages such as poor mechanical, thermal and adhesion properties. In this regard epoxy-silica hybrids offer enhanced properties combining the mechanical, thermal and chemical stability [1] of the siloxane-silica inorganic part and the processability and flexibility of the cured epoxy resin.

1.1 Epoxy-resins system

The most common epoxy-resins are based on Bisphenol A (BPA) and Bisphenol F(BPF) (Fig. 1). This system, characterized by two or more oxirane rings, has in general poor thermal, mechanical and chemical stability, properties which are significantly improved when a curing agent is added. Most curing agents, which provide a cross-linking of the Bisphenol segments, have functionality equal or superior of three ($f \geq 3$), f giving the number available bonding sites, like triethylene triamine (6 hydrogens prone to provide bond: $f = 6$) or Diamino diphenyl methane ($f = 4$) (Fig. 2). Curing agents proceed by a S_N2 nucleophilic attack to the less substituted carbon in the oxirane ring, resulting in its opening and in the formation of a OH group. This in turns results in the formation of a secondary amine, that even if it has a lower reactivity than a primary amine [2], attacks another epoxy ring resulting in a highly branched polymer system, known as a thermoset, that in contrast to a thermoplastic, has all its polymer chains linked together, explaining its high thermal stability [2]. As a highly reticulated hybrid structure is desired, the molecular weight for DGBEA was chosen to be low (380 g mol^{-1}) so the number-average degree of polymerization (DP_n) is equal to 0.1 (almost monomeric). For the

curing agent two criteria were considered: a curing agent with high functionality and small aliphatic chains. In this sense, diethyltriamine or DETA (Fig. 2) is the cross linker that best fulfills these requirements.

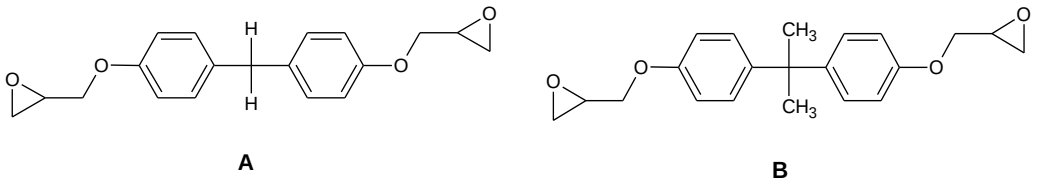

Fig. 1. Bisphenol F (A) and Bisphenol A (B) epoxy resins.

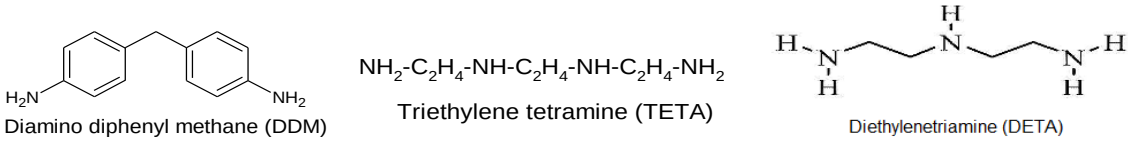

Fig. 2. Common curing agents.

1.2 Epoxy-silica hybrids

Organic-inorganic hybrids are part of a new class of materials that are defined as nanocomposites at the molecular level, having at least one component (either organic or biological) with a characteristic length scale on the nanometer size. This characteristic yields interesting mechanical, optical and thermal properties allowing a new range of applications, like drug delivery systems, optical and electrical devices, catalysis, photochromatic devices and protective coating systems, among others [3,4].

Organic-Inorganic hybrids can be divided into two classes according to the kind of interaction present between their constituents. In class I organic-inorganic hybrids, weak interactions (van der Waals, hydrogen and ionic) are present between the organic-inorganic components. A well-known example is maya blue, that is made of the natural indigo encapsulated within a clay mineral known as palygorskite. This material combines the color

of the organic pigment and the resistance of the inorganic host, a synergic material with properties well beyond those of a simple mixture of components.

Materials of main interest in this work present covalent bonds between the organic and inorganic phase. These systems, including epoxy-silica composites, are classified as type II organic-inorganic hybrids, in contrast to type I hybrids, lacking a strong interaction between its constituents. The most common methodology used for the preparation of hybrid materials is the sol-gel route, that compared with other methods does not require high temperatures, or extreme conditions for its synthesis and produces an homogenous material with a high degree of homogeneity and purity [3]. The sol is made-up of colloidal particles and dispersed polymeric chains, whereas the gel consists of interconnected structures (polymeric chains or aggregates), produced by polymerization and hydrolysis/polycondensation reactions, forming a rigid hybrid network. The formation of type II hybrids occurs when the organic and inorganic phases are linked together by a coupling agent, such as GPTMS (3-Glycidoxypropyl trimethoxysilane or GPTMS), containing a silica group linked by a Si-C bond to an epoxy tail. It is well known that silica-based inorganic materials prepared by the sol-gel method provide higher strength and thermal stability, but also a material with elevated porosity. The insertion of an organic compound into the pores of the inorganic structure produces a relatively hard and dense material that is thermally and mechanically resistant (inorganic characteristic) and slightly malleable, resulting in low internal stress (organic characteristic). This allows the preparation of stable and adherent films with thicknesses of several micrometers. The optimization of the hybrid structure, in terms of degree of polycondensation of the inorganic phase and the degree of cure of the organic phase, can be performed by the careful adjustment of the synthesis conditions, forming a hybrid matrix that is highly reticulated, resulting in a high thermal and mechanical stability, and in form of coating it acts as a hermetic barrier that is able to block the diffusion of corrosive agents. Several studies were realized by the GFQM group (Grupo Físico-Química de Materiais - IQ/UNESP) based on the PMMA-silica systems, using poly(methyl methacrylate) as the organic phase. The results have shown that the optimization of the synthesis parameters enables the preparation of hybrid films with a highly reticulated structure that provides a very efficient corrosion protection of metallic surfaces, showing a stability of more than 10 months in contact with a 3% NaCl solution [5]. Despite of this excellent performance, the main drawback of the PMMA-silica systems is its low thermal stability (<200°C), which is a critical parameter for several applications.

1.3 Sol-gel process

In the sol-gel process the precursors used for the preparations of colloids consist of metals or semimetals linked to several ligands, in the form of inorganic salts (chloride, nitrate, sulfate etc..) or alkoxides. An alkoxide is a ligand formed by the removal of one proton from a hydroxyl group of an alcohol, like a methoxy ($\cdot OCH_3$) or ethoxy ($\cdot OCH_2CH_3$). Metallic alkoxides are members of the family of organometallic compounds, containing at least one carbon atom of an organic compound bonded to the metal. Metallic alkoxides are widely used in sol-gel process due to their high reactivity with water, promoting a hydrolysis reaction (Fig. 3 I) where alkoxide groups (OR) are substituted by hydroxyl groups (OH), and the condensation reactions (Fig. 3 II and III), where Si-O-Si bonds are formed. The most used alkoxide is tetraethyl orthosilicate ($Si(OC_2H_5)$ or TEOS. [6][7]

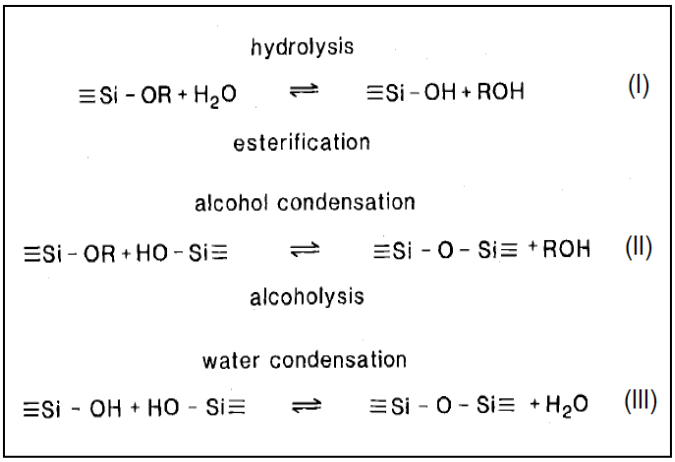

Fig. 3. Hydrolysis and condensation reactions in the sol-gel process, adapted [6]

The sol-gel transition is a phenomenon that occurs when clusters of colloids/polymers grow by condensation until they interact, then links are formed between the clusters until a single giant cluster is created that is called a gel. [6] The theory of gelation developed by Flory and Stockmayer gives a more precise description: the gel point is described by a decrease in the average molecular weight of the system, as the largest polymers become part of the growing cluster leaving the smaller polymers in the sol phase [6]. The gel-time, defined as the time that the systems takes to gel, is critical for the preparation of films as film deposition is only possible during the sol phase.

1.4 Justification

Epoxy-silica coatings offer a very promissory alternative compared to conventional corrosion inhibitors. They not only combine all the advantages of the epoxy resins but they also offer an improved adhesion to metallic substrates, and a higher thermal and mechanical stability. Hence, the study of this system is a promising research field, as only few studies [8] investigated the formation mechanisms between different precursor (TEOS, GPTMS, DETA and DGBEA) as a function of the sol-gel parameters. The success depends crucially on the understanding and control of the material's structural properties. Due to the enormous versatility of hybrid materials a number of different applications might be possible that go beyond the applications highlighted above. Recently epoxy-silica systems were applied in order to replicate neuronal cultures [9].

2 OBJECTIVES

- To determine the experimental variables that result in type II hybrids having a high degree of polymerization of the organic phase and a high degree of polycondensation of the inorganic phase.
- To correlate the structural characteristics with the thermal and anticorrosive properties of the films.

3 METHODOLOGY

The following reagents were used as received and are available commercially: tetraethylorthosilicate (TEOS, Aldrich), Poly(Bisphenol A-co-epichlorohydrin) (DGBEA, Sigma-Aldrich, M_n=324 g/mol, n=0.1), Diethyltriamine (DETA, Sigma-Aldrich), (3-Glycidoxypropyl)methyldiethoxysilane (GPTMS, Sigma-Aldrich) and Tetrahydrofuran (THF, Mallinckrodt)

The siloxane-epoxy hybrids were prepared by the sol-gel route in two stages: In the first step the epoxy resin (poly(Bisphenol A-co-epichlorohydrin)) (DGBEA) and (3-Glycidoxypropyl)trimethoxysilane (GPTMS) were cured with diethyltriamine (DETA) in THF during 4 h at a temperature of 70 °C under constant stirring in a reflux flask. In the second step TEOS, acidified water (pH 1) using nitric acid and ethanol was added to the reflux system at room temperature (25 °C) and stirred for an additional 1 h. At this stage the

modified GPTMS is partially hydrolyzed and condensed with TEOS, forming a homogeneous and transparent sol used for the deposition of films by dip-coating,

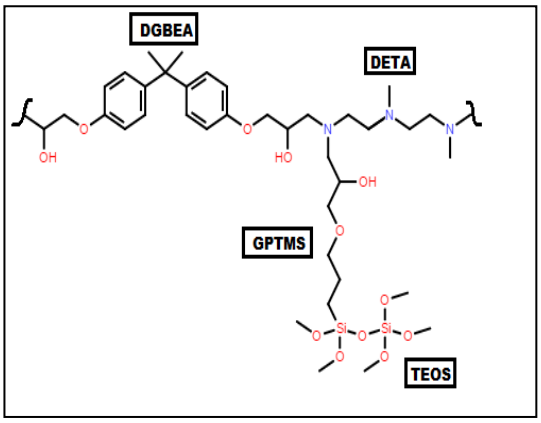

Fig 4. Idealized structure of the building blocks of the siloxane-epoxy hybrid.

3.1 Synthesis of epoxy silica hybrids

A 1010 carbon steel (25 mm x 20 mm x 5 mm) has been used as substrate, having a nominal composition (wt%) of C = 0.08 to 0.13%, Mn = 0.3 to 0.6%, P_{max} = 0.04% and S_{max} = 0.05%, with the balance consisting of Fe. The deposition of hybrid films was performed by dip-coating (Microchemistry—MQCTL2000MP) at a rate of 14 cm min^{-1}, with 1 min of immersion and air-drying during 10 min at room temperature. This procedure was performed three times for each sample. Then the coated substrates were cured at 60 °C for 48 h. Two series of hybrids with varying GPTMS and TEOS ratios were prepared: GPTMS/TEOS/DGBEA = 0.5/1/1; 1/1/1; 1.5/1/1; 2/1/1; 2.5/1/1, and TEOS/GPTMS/DGBEA= 0/1/1; 0.5/1/1; 1/1/1; 1.5/1/1; 2/1/1; 2.5/1/1, referred to as G_ 0.5, G_1, G_ 1.5, G_ 2, G_ 2.5 and T_0, T_0.5, T_1, T_1.5, T_2, T_2.5, respectively (Fig. 5). In order to ensure a fully cured thermosetting, DETA was added in a proportion that resulted in one oxirane group for every hydrogen atom of the amine groups.

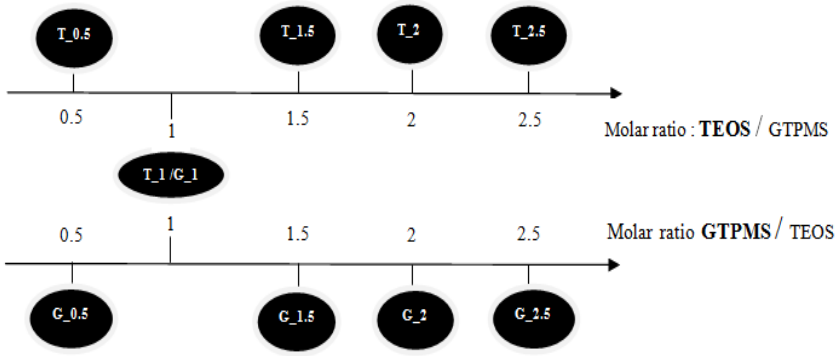

Fig 5. Naming of the different samples according to the molar TEOS/GPTMS ratio.

3.2 Characterization Techniques for epoxy silica hybrids

In the first part of the project the structural characterization of the epoxy-siloxane-silica hybrid has been performed using Raman, infrared spectroscopy, X-ray photoelectron, small angle X-ray scattering and ^{29}Si Solid NMR spectroscopy.

The hydrophobicity of the hybrid is assessed by contact angle measurements, the thermal stability was studied by thermogravimetry (TG) and finally the anticorrosive performance of the coated carbon-steel samples was tested using electrochemical impedance spectroscopy (EIS). The film thickness is determined by optical interferometry system (FILMETRICS).

3.2.1 Microscopies

Reflected light microscopy has been used in order to verify the homogeneity of the film. A XJM900 Metallurgical microscope, installed at GFQM (IQ/UNESP), was used.

Scanning electron microcopy (SEM) was performed to characterize the surface morphology of films. A 7500F field emission gun transmission electron microscope (FEG-SEM) equipped with a Brucker energy dispersive X-ray spectroscopy (EDX) was used (IQ/UNESP).

The surface topography of the films in terms of roughness was determined by Atomic Force Microscopy. Agilent 5500 Technologies model, in the tapping mode, with a silicon cantilever, installed at GFQM, was used. From 1 μm^2 topographic images of the hybrid films deposited on carbon steel, the RMS roughness (Root Mean Square) was calculated from the standard deviation:

$$\mathrm{RMS} = \sqrt{\frac{1}{N-1}\sum_{i=1}^{N}(x_i - \overline{x})^2}.$$

where $\overline{x}$ is the arithmetic mean of the x values inside the area of the image, is the value of x and N is the number of points.

3.2.2 X-ray photoelectron spectroscopy (XPS)

XPS was used in order to determine the elemental composition of the hybrids as well as the chemical bonding structure of carbon (C 1s) , oxygen (O 1s), nitrogen (N 1s) and silicon (Si 2p). The analysis were carried out at a pressure of less than 10^{-7} Pa using a commercial spectrometer (UNISPECS UHV). The Al Kα line was used (hν = 1486.6 eV) and the pass energy for the higher solution spectra was set to 10 eV. The inelastic background of the C 1s, O 1s, N 1s and Si 2p electron core-level spectra was subtracted using Shirley's method. The composition of the near surface region was determined with an accuracy of ±10% from the ratio of the relative peak areas corrected by Scotfield's sensitivity factors of the corresponding elements. The spectra were fitted without placing constraints using multiple Voigt profiles.

3.2.3 Micro-Raman spectroscopy

Raman spectroscopy was used in order to identify the main functional groups present in the hybrid film, as well as to verify the opening of the oxirane ring by the amine moieties and the formation of the silica network. A Lab RAM HR 800 (Horiba Jobin-Yvon) spectrometer was used, installed at IQ/UNESP. A He-Ne laser with excitation line of 632 nm was used as light source. The spectra were recorded in the range of 400 to 3500 cm^{-1} using a silicon line for calibration.

3.2.4 Fourier Transform Infrared spectroscopy (FTIR)

FTIR was used to determine the degree of cure of the epoxy resin. For a vibrational mode to absorb IR radiation the frequency of the incoming beam must match the vibrational frequency of the mode with electrical field interacting with the molecule's permanent dipole moment. The analyses were carried out in a Vertex 70/BRUKER FTIR installed at IQ/UNESP using the attenuated total reflectance (ATR) mode.

3.2.5 Small X-ray angle scattering (SAXS)

SAXS measurement were performed to determine the nanostructural characteristics of the hybrids. The measurements were carried out at the synchrotron SAXS beamline of the National Synchrotron Light Laboratory (LNLS, Campinas, Brazil). The SAXS beamline is equipped with an asymmetrically cut and bent silicon (111) monochromator that yields a monochromatic (λ = 1.608 Å) and horizontally focused beam. A vertical position sensitive X-ray detector and a multichannel analyzer were used to record the SAXS intensity, I(q), as a function of the modulus of the scattering vector q, $q = (4\pi/\lambda) \sin(\Theta/2)$, Θ being the scattering angle.

In the low q region, the scattering intensity produced by dilute particles dispersed in a homogeneous matrix is described by the Guinier law:

$$I(q) = G \exp(-q^2 R_g^2/3) \qquad \text{Eq. 1}$$

Where G is dependent on the difference between the average electron density between the matrix and the scattering particles, and R_g is the radius of gyration of the particles. In the high q region the scattering intensity is given by the Porod law:

$$I(q) = A\, q^{-p} \qquad \text{Eq. 2}$$

Where $A = 2\pi \Delta p^2 S$, Δp being the difference in electronic density and S the interface area between the particle and the matrix. The exponent p is related to the geometry and the sharpness of the interface of the particles, in the case p = 4 the surface of the particle is smooth whereas for values $1 < p < 3$ it show a fractal character. [10]

Beaucage proposed a unified semi empirical equation, describing the scattering intensity for not interacting particles in the low and high q region by the following expression [11]

$$F(q) = G\exp\left(\frac{-q^2 R_g^2}{3}\right) + B\left[\frac{\left(erf\left(\frac{qR_g}{2.499}\right)\right)^3}{q}\right]^P \qquad \text{Eq. 3}$$

The *erf* function or error function acts as a cut off function bringing to zero the Porod law contribution.

In the case of concentrated particles where Eq. 3 non longer holds i.e. the scattering intensity is no longer described by the sum of the contribution of each particle but interferences need to be taken into account. In this case the structural form factor is introduced and the total intensity for center-symmetry is described by the product of Eq. 4 and the structural and form factor F(q):

$$I(q) = F(q) * S(q) \qquad \text{Eq. 4}$$

Beaucage [11] used the Born-Green theory and proposed a simple expression for the structural form:

$$S(q) = 1/(1 + k\theta) \qquad \text{Eq. 5}$$

Where k, the packing factor, is related to the number of neighboring particles and θ, the form factor, which depends on the interparticle distance.

Under these assumptions it is possible to describe the scattering intensity for a two level system i.e a system described by (level 1) in (level 2), using the following expression [12]:

$$I(q) = \left[G_1\exp\left(\frac{-q^2 R_{g_1}^2}{3}\right) + B_1\left[\frac{\left(erf\left(\frac{qR_{g_1}}{2.449}\right)\right)^3}{q}\right]^{P_1}\right]\cdot S_1(q) + \left[G_2\exp\left(\frac{-q^2 R_{g_2}^2}{3}\right) + B_2\exp\left(\frac{-q^2 R_{g_1}^2}{3}\right)\left[\frac{\left(erf\left(\frac{qR_{g_2}}{2.449}\right)\right)^3}{q}\right]^{P_2}\right]\cdot S_2(q) \qquad \text{Eq. 6}$$

Where R_{g1} and R_{g2} is the radius of gyration of the silica nanoparticles and of the clusters of silica respectively.

3.2.6 Nuclear magnetic resonance (NMR)

^{29}Si solid NMR measurements allowed the identification of the local Si bonding structure and in particular the determination of the degree of poly-condensation of the inorganic phase. A solid-state ^{29}Si magic-angle spinning nuclear magnetic resonance (MAS-NMR) was employed the spectra were recorded for powder samples using a VARIAN spectrometer operating at 300 MHz and 7.05 T. The Larmor frequency for ^{29}Si and ^{13}C was 59.59 Hz and 75.42 Hz, respectively. The spectra were obtained from the Fourier transformation of the free induction decays (FID), following a single $\pi/2$ excitation pulse and a decay time of 2 s. Chemical shifts were referenced to tetramethylsilane (TMS) and MMA, used as external standards. Proton decoupling was always used during acquisition of the spectra.

3.2.7 Contact angle measurements

Measurement of the equilibrium contact angle between the liquid and the material were performed to determine the wettability of the hybrid film and to assess the dispersive character of the hybrid's surface. The equilibrium contact angle and the hybrid's surface tension are given by the Young equation:

$$\cos(\Theta_y) = (\gamma_{sv} - \gamma_{sl}) / \gamma_{lv} \qquad \text{Eq. 9}$$

Where Θ_y is the Young contact angle and γ_{sv}, γ_{sl} and γ_{lv} are the surfaces tensions between the solid-vapor, solid-liquid and liquid-vapor interfaces (Fig. 6). In the case of a nearly perfect flat surface (which is the case of our deposited films) Θ_y can be equated to the measured contact angle (Θ_m) and directly relate Θ_m to the hydrophobicity of the material (Fig. 5) i. e. the higher Θ_m the more hydrophobic is the material. In order to determine the dispersive content of the hybrid material Eq. 9 has to be combined with the Dupre equation [13,14]:

$$(1 + \cos(\Theta_m)) / 2 \ast \gamma_{lv} / (\gamma_{lv}^d)^{0.5} = (\gamma_{sv}^p)^{0.5} \ast (\gamma_{lv}^p / \gamma_{lv}^d)^{0.5} + (\gamma_{sv}^d)^{0.5} \qquad \text{Eq. 10}$$

Where γ_{lv}^d and γ_{lv}^p are the dispersive and polar components of the liquid surface tension. If $(1+\cos(\Theta_m)) / 2 * \gamma_{lv} / (\gamma_{lv}^d)^{0.5}$ is plotted against $(\gamma_{lv}^p / \gamma_{lv}^d)^{0.5}$ and fit the points to a straight line we can determine the polar (γ_{sv}^p) and dispersive (γ_{lv}^d) surface tension of the hybrid material. All the measurements were performed in a OCA, DATAPHYSIC system, coupled with a CCD camera, with the help of a SCA20.2.0 software, installed at GFQM.

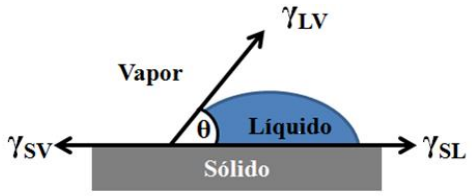

Fig. 6. Representation of the surface tensions and contact angle, adapted from [15].

3.2.8 Thermogravimetry (TG)

Thermogravimetry enables the study of the thermal stability of the material monitoring the decomposition of the material by the mass loss as a function of temperature, as well as the determination of the organic part of the hybrid from the residue at high temperature. TG curves of the hybrids where obtained using a TA instrument SDT Q600 equipment at GFQM (IQ/UNESP). The following conditions were used: nitrogen or oxygen atmosphere with a continuous flux of 70 mL min^{-1}, the mass of the sample was of 7 mg in an alumina crucible, the temperature range was from 25 to 800 °C, at a heating rate of 10 °C min^{-1}.

3.2.9 Electrochemical impedance spectroscopy (EIS)

The corrosion protection efficiency of the hybrid films deposited in carbon steel has been studied using EIS as a function of time of immersion in a saline solution. The measurements were carried out in an electrochemical cell at 25 °C in a 80 mL solution containing 3.5% of NaCl (Fig. 6), after verifying the value of the open-circuit potential (E_{oc}) for 5 min a 10 mV_{rms} sinusoidal potential was applied. The frequency was then varied from 300 kHz to 5 mHz using a Potentiostat/Galvanostat GAMRY REFERENCE 600, installed at GFQM.

The principle of this technique consists in applying a sinusoidal potential, and recording the alternating current and thus the impedance of the electrochemical system. The impedance $Z(\omega)$, has a real and imaginary part, represented by a vector with modulus $|Z|$, where $|Z| = (Z_{real} + Z'_{img})^{1/2}$. The angle between the vector $|Z|$ and the x-axis is known as the phase angle φ.

Working electrode: coated carbon steel
Reference electrode: Ag | AgCl | KCl_{sat}
Counter electrode: Platinum grid
4° electrode: Platinum
Capacitor: 0.1μF
Solution: NaCl 3.5%

Fig. 7 . Electrochemical cell in a faraday cage used for EIS measurements.

4 RESULTS AND DISCUSSION

4.1 Structural and morphological analysis

4.1.1 Morphological analysis

Fig. 8 and 9 show representative images of the surface morphology, obtained by optical microscopy and AFM of the G_1.5 and T_1.5 hybrid coatings and the bare carbon steel. Micrographs showed for all samples a homogenous and transparent film with no heterogeneities at the micrometric scale. AFM showed that the surface roughness (R_{rms}) of the samples, calculated as an average of a 1 μm^2 area, increases when GPTMS and TEOS content is increased, from 0.6 nm for G_0.5 to 1.4 nm for G_2.5 and from 0.3 nm for T_0.5 to 4.9 nm for T_2 (Table 1).

The data suggest that increasing concentrations of TEOS has a larger impact on the surface roughness than that of GPTMS, probably due to the formation of silica domains of increasing size. FEG-SEM images show the surface morphology of the T_0.5, T_2 and T_2.5 films (Fig. 10). The presence of localized elevations (white spots) increases with increasing TEOS concentration, which in agreement with the tendency of R_{rms} values, determined by AFM. Thus they can be related to the localized elevations, observed in AFM except for the T_2.5 sample, suggesting that each of these elevations have a width of approximately 9 nm and a height of 1 to 3 nm.

Measurements of the thin films thickness showed for all samples of the G-series a constant value of about 1.7 μm. For the films of the T-series, T_1.5 has a thickness of 6.7 nm, while the other coatings have between 2 to 3 μm. Table 1 summarizes the principal morphological and optical features of the films.

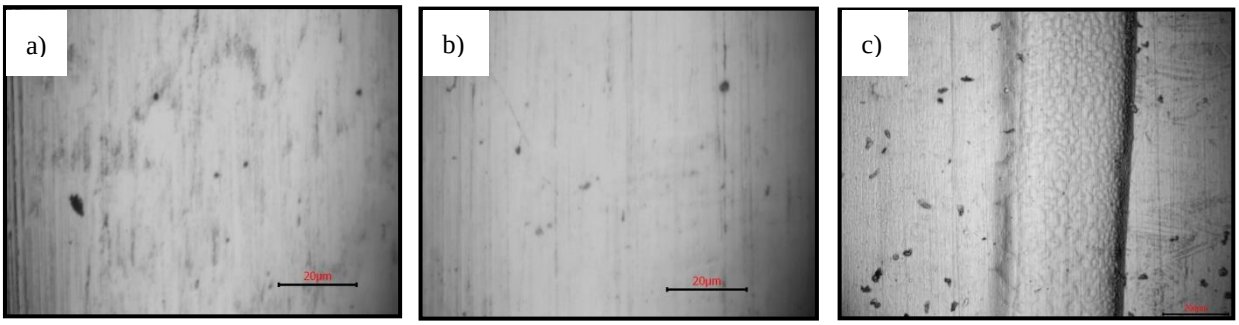

Fig. 8. Optical micrograph of the G_1.5 film (a), carbon steel (b) and the interface between the T_1.5 film and the carbon steel (c).

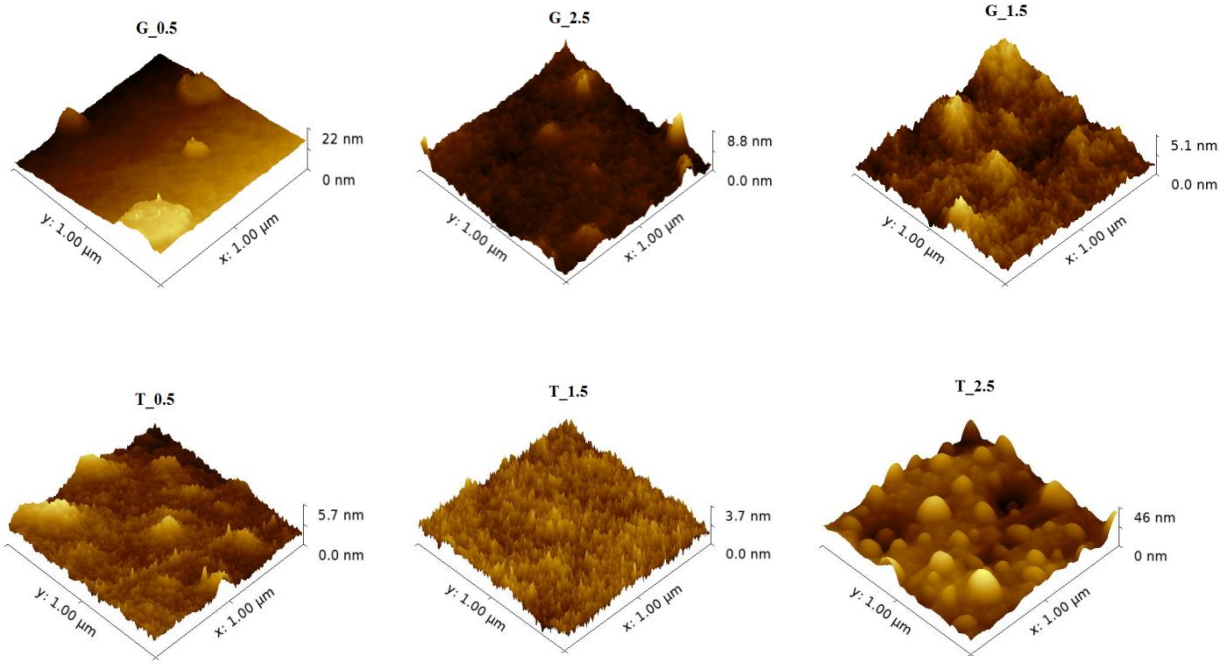

Fig. 9. AFM surface morphology of the different hybrid coated carbon steel samples.

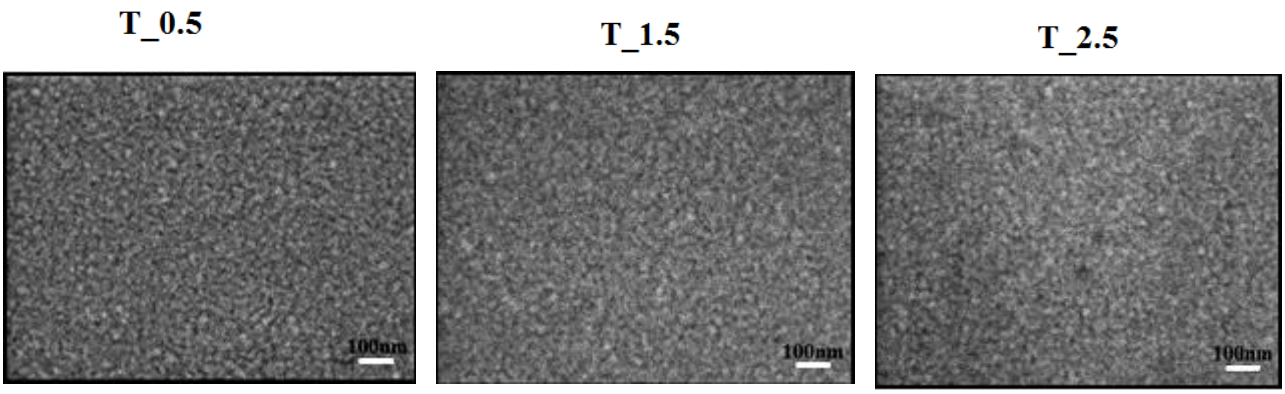

Fig. 10. Scanning electron microscopy (FEG-SEM) images of surface morphology of the T_0.5 , T_1.5 and T_2.5 samples.

Table 1. Main morphological and optical features of the films.

	T_0	**T_0.5**	**T_1.5**	**T_2**	**T_2.5**	**G_0.5**	**G_1**	**G_1.5**	**G_2**	**G_2.5**
RMS (nm)	0.34	0.68	0.33	2.6	4.94	0.6	1.21	0.43	1.02	1.38
Thickness (μm)	3.0	2.0	6.7	3.3	1.8	1.8	1.6	1.8	1.6	1.8
Film appearance	Uniform	uniform	uniform	Non-uniform	Non-uniform	uniform	uniform	Uniform	uniform	uniform
Interference pattern	Yes	Yes	No	No	No	Yes	Yes	Yes	Yes	Yes

4.1.2 XPS analysis

Table 2 and Table 3 show that results of the quantitative XPS analysis are in good agreement with the nominal composition for sample of both series. As expected, the data show an increase of silicon, nitrogen, and oxygen atomic concentration for the G series. It can be observed an increase of Si from 4.8 at.% (G_0.5) to 6.5 at.%Si (G_2.5), N from 2 at.% (G_0.5) to 2.8 at.% (G_2.5) and for O from 25.5 at.% (G_0.5) to 28.1 at.% (G_2.5). For the T series the atomic concentration of silicon increases from 3.2 at% (T_0.5) to 7.5 at% (T_2.5) and for oxygen from 22.9 at% (T_0.5) to 28.3 at%(T_2.5). As the structure of GPTMS contains carbon atoms its addition leads to a less pronounced increase of the Si content (decrease of the C/Si ratio) than in the case of TEOS.

Table 2. Comparison between XPS and calculated atomic percentages for the G series.

	G_0.5 XPS	Calculated Nominal percentage	G_1 XPS	Calculated Nominal percentage	G_2 XPS	Calculated Nominal percentage	G_2.5 XPS	Calculated Nominal percentage
	(at.%)*							
Si 2p	4.8	4.3	5.2	4.8	6.0	5.6	6.3	6.0
C 1s	67.7	71.3	67.6	68.4	66.2	65.3	62.7	65.6
O 1s	25.5	22.0	30.0	24.0	25.5	26	28.1	25.0
N 1s	2.0	2.5	2.2	2.8	2.3	3.3	2.8	3.5
C/Si	14.1	16.9	14.1	14.3	11.0	11.8	10.0	11.0

*Experimental error: ±5%

Table 3. Comparison between XPS and calculated atomic percentages for the T series.

	T_0.5 XPS	Calculated Nominal percentage	T_1.5 XPS	Calculated Nominal percentage	T_2 XPS	Calculated Nominal percentage	T_2.5 XPS	Calculated Nominal percentage
	(at.%)*							
Si 2p	4.4	3.72	5.9	5.77	6.8	6.69	7.5	7.55
C 1s	70.1	70.96	66.5	66.05	63.1	63.83	62.1	61.77
O 1s	22.9	22.33	25	25.40	28.3	26.78	28.1	28.077
N 1s	2.5	3	2.6	2.77	1.8	2.6	2.4	2.59
C/Si	15.9	19	11.3	11.44	9.3	9.5	8.3	8.1

*Experimental error: ±5%

Figure 11 compares the deconvoluted XPS Si 2p spectra for G_0.5, G_2.5 and T_0.5, TG_2.5 samples. For the G series the C-SiO_x component at 102.5 eV increases while the absolute area of the SiO_2, related to TEOS (103.3 eV) remains unchanged (Fig. 10 a). Whereas for the T series, the increase in silicon comes from TEOS, where the area of the C-SiO_x component remains unchanged, while the area of SiO_2 increases (Fig. 10b) proportional to the TEOS addition. As expected, G_1 and T_1 sample with GPTM/TEOS ratio of 1 show equal intensities of the SiO_2 and C-SiO_x components. Furthermore, as the organic phase

remained essentially unchanged for all samples, the deconvoluted C 1s spectra (Fig. 12a) shows constant intensities for the three components related to the bonding environment of carbon: C-C bonds at 294.7 eV, C-N bonds at 295.6 eV and C-O groups at 286.5 eV. The O 1s spectra shows only one component related to the superimposed intensities of the O-Si and O-C bonds at 532.7 eV (Fig. 12b).

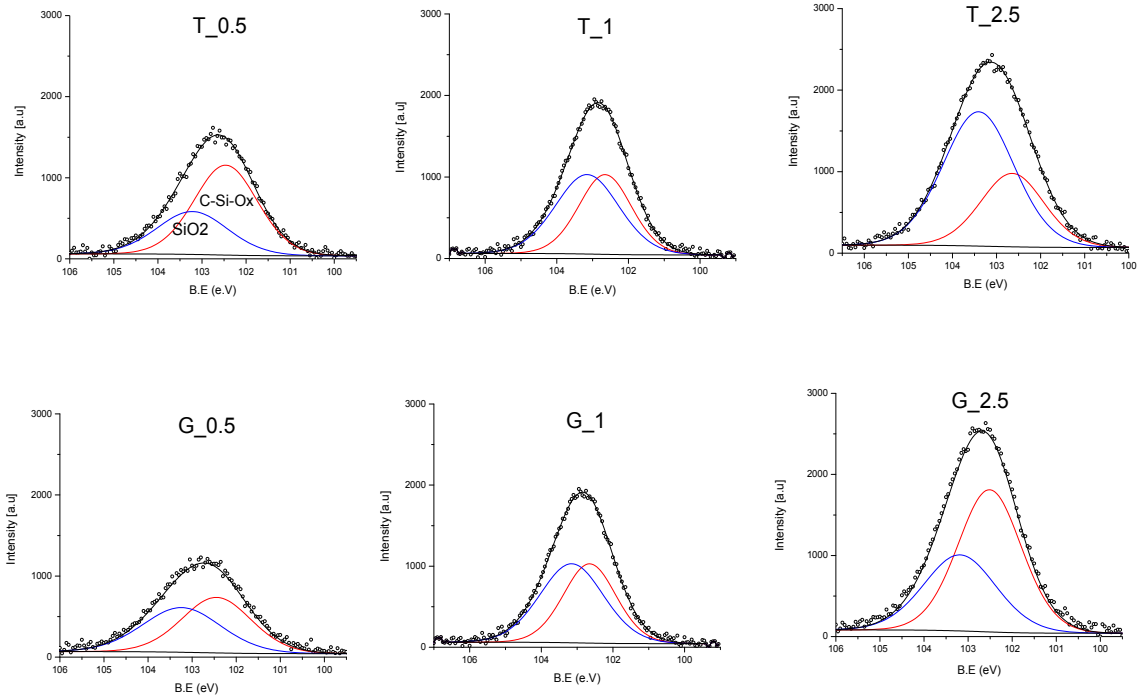

Fig. 11. Deconvoluted Si 2p spectra, showing the SiO_2 component of TEOS and the C-Si-O_x component of GPTMS for six different samples.

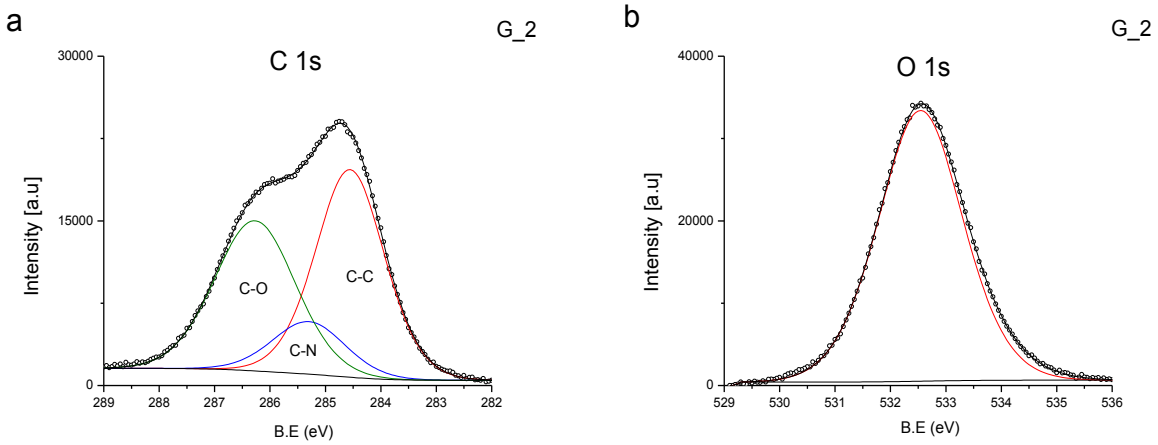

Fig. 12. a) Deconvoluted C 1s spectra, showing the components related to the carbon environment b) Deconvoluted O 1s spectra, shows only one component that correspond to superimposed intensities of the O-Si and and O-C bonds.

4.1.3 Raman and infrared structural characterization

The main vibrational modes identified in the hybrid film (G_1.5) by Raman spectroscopy are listed in the inset of Fig. 13. It is important to note that all samples have very similar spectra and that all peaks identified in Fig.13 for films are also present in the Raman spectra of the monoliths.

The presence of the siloxane bridge stretching vibration (475 cm^{-1}) evidences the formation of the silica network by the hydrolytic condensation reactions of the inorganic reagents. The stretching vibrations in the phenyl ring (1610 cm^{-1}), of phenylic hydrogen (3068 cm^{-1}) and methyl groups (2922 cm^{-1}) account for the presence of DGBEA. The primary and secondary amine stretching vibrations (738 and 823 cm^{-1}) as well as the methylene bridge stretch and waging vibrations (1461 and 2872 cm^{-1}) are indicative for the presence of DETA and the formation of methylene bridges by the opening of the oxirane ring by the amine moieties. Finally the oxirane ring and methylene stretching vibrations (1226 and 2955 cm^{-1}) show the presence of residual epoxy groups present in DGBEA and GPTMS

As complementary method FT-IR spectroscopy (Fig 14) was performed for all samples, showing characteristic peaks corresponding to DGEBA ($C=C_{aromatic}$ and phenyl hydrogen stretch at 1612 and 3008 cm^{-1}) and the aliphatic groups ($C(sp^3)$-H at 2900 - 3000 cm^{-1}). In contrast to Raman the FT-IR spectra show a broader band at 3381 cm^{-1}, a narrow band at 1036 cm^{-1}, and a weak band at 912 cm^{-1} accounting for the stretching vibration of O-H, C-O-C_{ether} and C-O deformation of the oxirane ring, respectively [16]. This lies in the fact that O-

H bonds are weak Raman scatterers but strong infrared absorbers and that C-O-C_{ether} vibration and C-O deformation of the oxirane ring are IR but not Raman active [17].

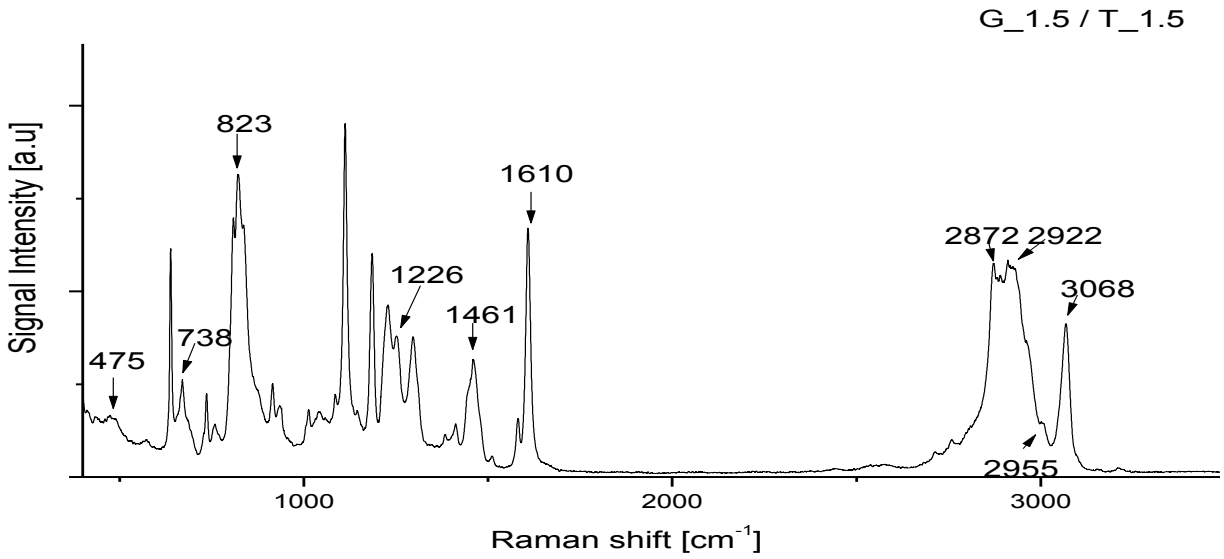

Mode	Si-O-Si	-NH_2 (stretch)	-NH- (stretch)	C-O-C (oxirane)	CH_2-N (stretch)	Phenil ring (stretch)	CH_2-N (stretch)	-CH_3 (stretch)	C-O-C-H_2 (oxirane stretch)	Phenil-H (stretch)
Raman shift (cm^{-1})	475	738	823	1226	1461	1610	2872	2922	2955	3068

Fig. 13. Raman spectrum obtained for the G_1/T_1 hybrid film (Inset: Attribution of principal bands (cm^{-1})).

However no bands corresponding to the silica network and the amine moieties were observed in the IR spectra. This is due to the fact that DGEBA has a very strong band at 1032 cm^{-1} (corresponding to the ether stretching), which overlaps with the Si-O-Si stretching band (1050 cm^{-1}) and the bands corresponding to the scissoring and wagging vibration of amines (3400-3500 cm^{-1} for primary amines and 3300-3400 cm^{-1} for secondary amines) are not only weak but also overlap with the broader band of the O-H bond. Hence, more information regarding the opening of the oxirane ring can be obtained using Raman than Infrared spectra.

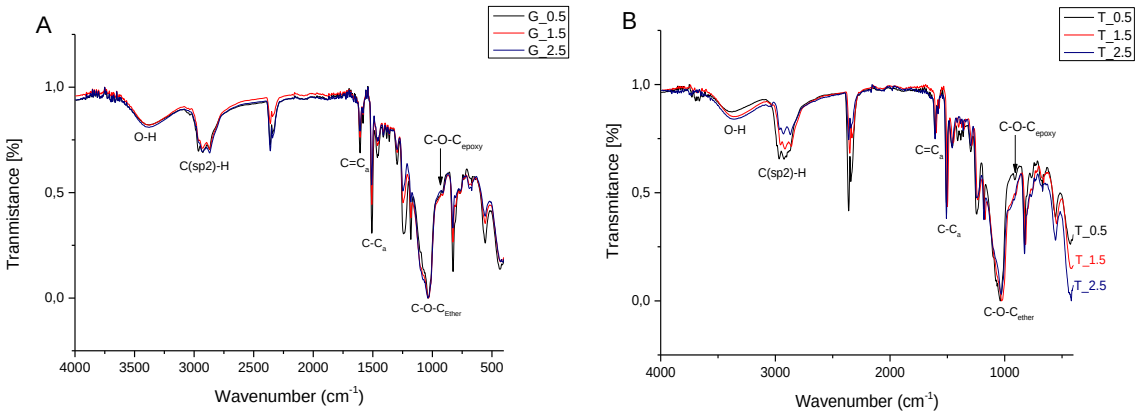

Fig. 14. FT-IR spectra obtained for the G series (A) and T series (B).

4.1.4 Epoxy conversion and opening of the oxirane ring

The curing reaction was monitored using Raman spectroscopy. For this purpose two vibrational modes can be used: the oxirane ring (1226 cm^{-1}) and methylene (2955 cm^{-1}) stretching vibrations. Two samples were compared: one where DETA was added (G1) and another where DETA was absent ($G1_{uncured}$), apart from DETA all molar quantities of the other reagents were kept constant. Figure 15 clearly shows that the bands corresponding to the stretching vibrations of the oxirane ring have lower intensities for the cured (G1) sample than that of the uncured sample ($G1_{uncured}$), suggesting the opening of the oxirane ring and a preferential attack of the amine moieties to the least substituted carbon of the ring. It is also interesting to note, that the deconvoluted XPS N 1s spectra (Fig. 16) of all hybrids show

nitrogen mainly in the form of a tertiary amine (399.2 eV), confirming once again the opening of the oxirane ring, with a small fraction of N having a lower electronic density (401.5 eV) probably corresponding to a protonated amine, which is expected since acidic water was used during the synthesis of the hybrid.

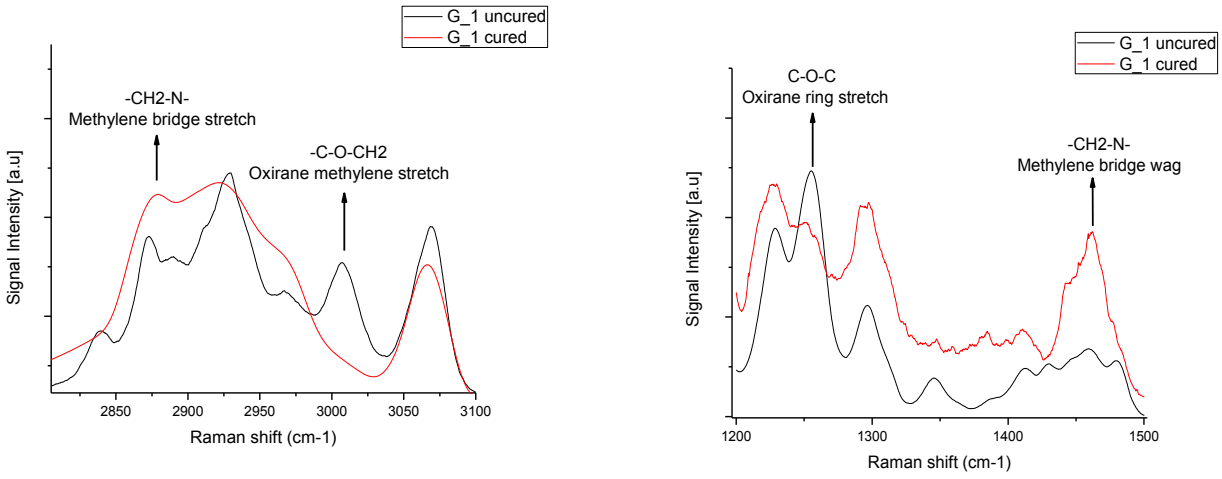

Fig. 15. Raman spectra of the uncured and cured G_1 hybrid film showing the opening of the epoxy ring.

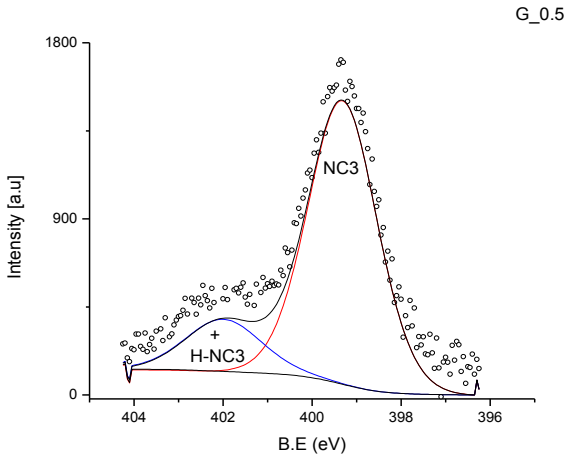

Fig. 16. Deconvoluted N1s XPS spectra for the G_05 sample showing the presence of N mainly in the form of tertiary amine at lower binding energy and as protonated amine at higher binding energy.

The extent of the curing reaction in terms of epoxy conversion (fraction of epoxies that have reacted) was determined using the FT-IR spectra by integration of the epoxy band at 912 cm^{-1} and the C-C_a band (1508 cm^{-1}) as the band of reference, using the following expression [16]:

$$\alpha_e = (A_{non\ cured} - A_{cured}) / A_{non\ cured} \quad \text{Eq. 11}$$

Where $A_{non\ cured}$ is the normalized area of the epoxy band at 912 cm^{-1} for a non-cured hybrid and A_{cured} is the normalized area of this band for a cured hybrid. The epoxy conversion percentages obtained for samples of the T series, as listed in Table 2. The results show similar epoxy conversions that range from 82% for T_ 0.5 to 89% for T_2.5. This increase can be explained by the increasing amounts of acidic water used during the synthesis. This results, besides the protonation of a fraction of amine groups, in an increase of the number of protonated epoxy rings, making the less substituted carbon of the ring behave like a carbocation, thus being more prone to react.

Table 4. Epoxy conversion for the hybrid samples.

	T_0	T_0.5	T_1.5	T_2	T_2.5
Epoxy conversion α_e (%)	82	83	85	89	89

4.1.5 Structural characterization of the inorganic network

The presence of bending vibration of the siloxane bridge (Si-O-Si) at 485 cm^{-1} in the Raman spectra (Fig. 16) as well as the absence of the ethoxy vibration (-O-CH_2CH_3) at 1075 cm^{-1} corresponding to GTPMS in the IR spectra show the formation of the silica network. For the G series the signal-to-noise ratio for the Si-O-Si signal in the Raman spectra decreases as the concentration of GPTMS increases, whereas the opposite trend is observed for the T series (except for T_2.5). Davis and Atkins [18] observed that the formation of one network has a considerable influence in the formation of the other, perhaps explaining the trend

observed in the G series, where higher concentrations of GPTMS result in a more robust organic part, thus constraining the formation of the inorganic part.

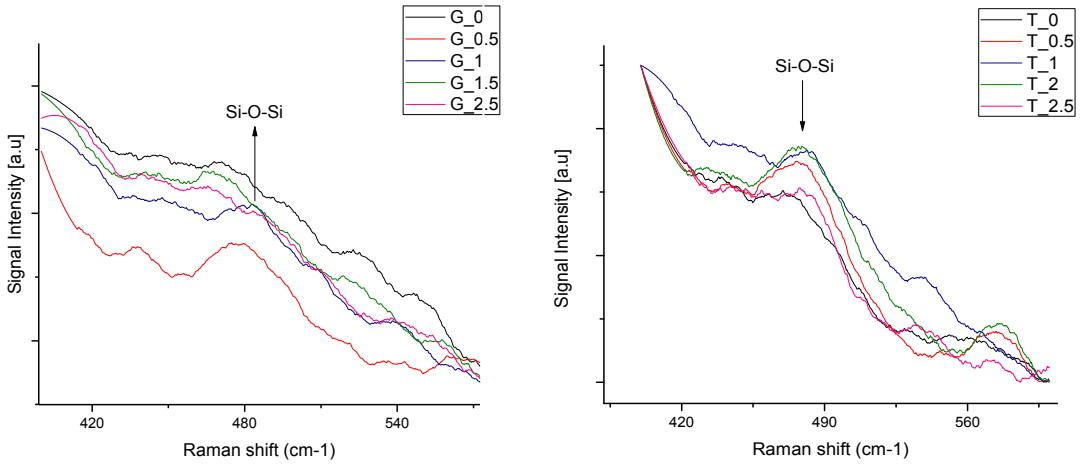

Fig. 17 Raman spectra showing the formation of the oxide network for the G and T series

The nanostructural characteristics of the inorganic network of the T series have been investigated by small angle X-ray scattering (SAXS). The scattering curves of Figure 18 show two regimes: one at lower q range ($q < 0.4$ nm^{-1}) showing a decreasing intensity and the other at higher q range, presenting a large peak in the range of $1 < q < 1.2$, related to correlation between particles. This scattering pattern has been observed in other silica-polymer hybrids [19][20] and has been associated with a two level system, corresponding to two interrelated structural features at different scales embedded in a polymer matrix.

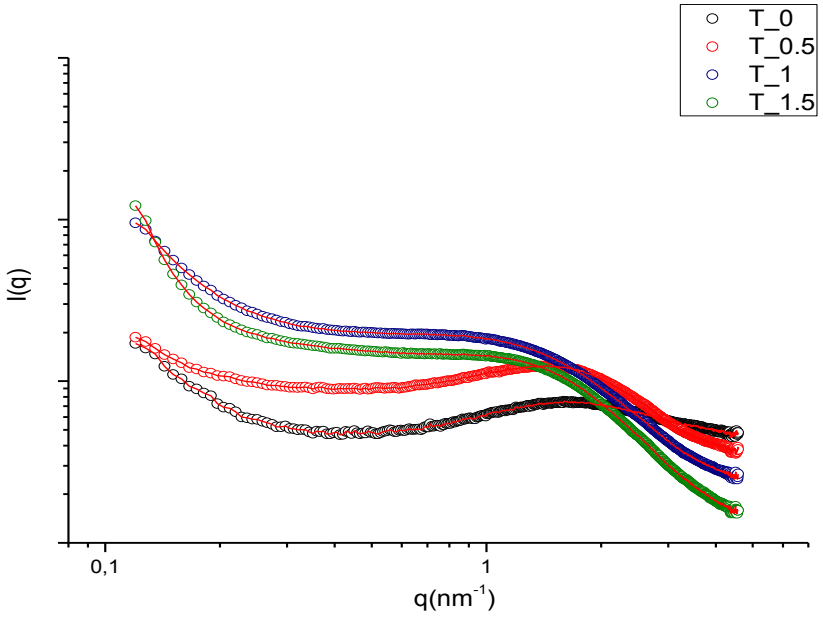

Fig. 18. Log-Log plot of the scattering Intensity as a function of q for the T series. The red lines are fitted curves obtained from Eq 6.

Using the unified Beaucage equation (Eq. 6) it is possible to fit the data points as shown in figure 16. The good agreement between the fitted curve and data points (chi values (χ^2) of less than 10^{-3}) supports the existence of a two level system of silica particles, forming the inorganic phase. Unfortunately, due to the limitation of data for small q values (absence of level 2 Guinier plateau for all the samples and of a level 1 Guinier plateau, for the T_0 and T_0.5 samples) several parameters obtained from Eq. 6 do not provide reliable values.

Alternatively P_1, the Porod coefficient, and R_{g1}, the radius of gyration from level 1 particles, were determined by using the Guinier and Porod fitting. The correlation distance, d_1, was calculated by determining q_{max} for T_0 and T_1 using the following relation $d_1 = 2\pi/q_{max}$. The different parameters are listed in table 5.

Table 5. R_{g1}, d_1 and P_1 for the T series samples

	T_0	T_0.5	T_1	T_1.5
R_{g1}(nm)	-	-	0.81	0.81
d_1 (nm)	3.76	4.13	-	-
P_1	-	0.81	1.03	1.41

The P_1 values for all the samples are close to -1 indicates a fractally rough (irregular) interface for domains of both levels. The value of Rg_1 for T_1 and T_1.5 sample is about 0.8 nm, this is expected since the nominal percentage is relatively low (Table 3) and the difference between both samples is only 0.5%. Since no relation is observed between the width of the white spots (~9 nm) observed in SEM and Rg_1 being very small, they can be related to the clusters of Silica (level 2 structures), however the lack of Rg_2 values, difficults to confirm the relation between SAXS and SEM data. Fig. 19 shows a representation of the inorganic phase based on the data shown in Table 5

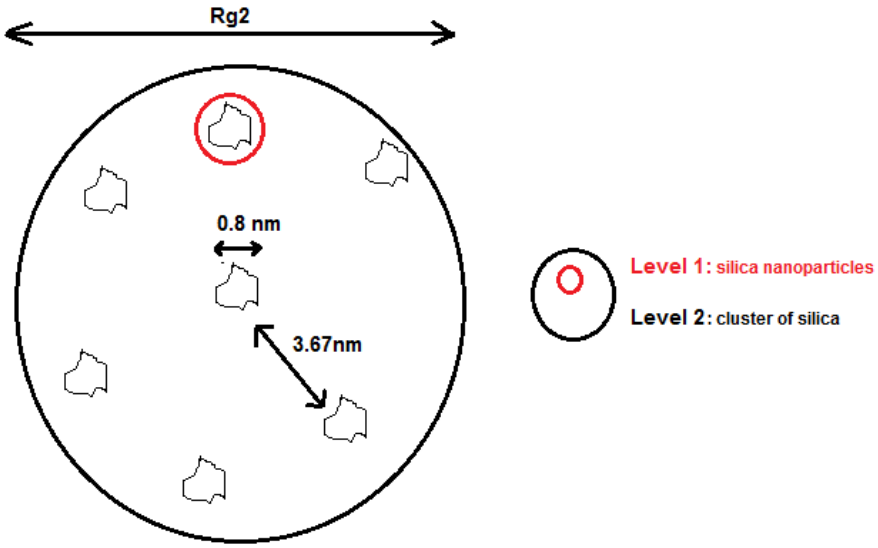

Fig. 19. Suggested nanostructure of the inorganic network. The large circle (in black) represents the Level 2 silica cluster, while the small circle (in red) represent the silica nanoparticles.

The increase of TEOS content is accompanied by the disappearance of the correlation peak as seen in Figure 17, indicating an increase in the distance between the nanoparticles. Although it is not possible to explain this tendency with accuracy given the limited data range, some models have been proposed, and in particular the chain-end model seems to match the experimental observations.

This model assumes that the end to end distance for a polymer is proportional to its molecular weight, based on this assumption it is possible to understand how increasing concentrations of TEOS results in uncorrelated particle system. Since the molecular weight of DGBEA is low (n=1), two Si-OH groups from two different GPTMS molecules are close enough, so when the silica phase is formed they start to interact. In fact, the distance between two ends, using a very simplified model (Fig. 19), is around 3 nm which is in accordance with the d_1 distances found for the T_0 and T_05 samples (Table 5).

However when TEOS is added the Si-OH group is no longer the privileged site of nucleation, and several sites form throughout the film, explaining the disappearance of the correlation peak.

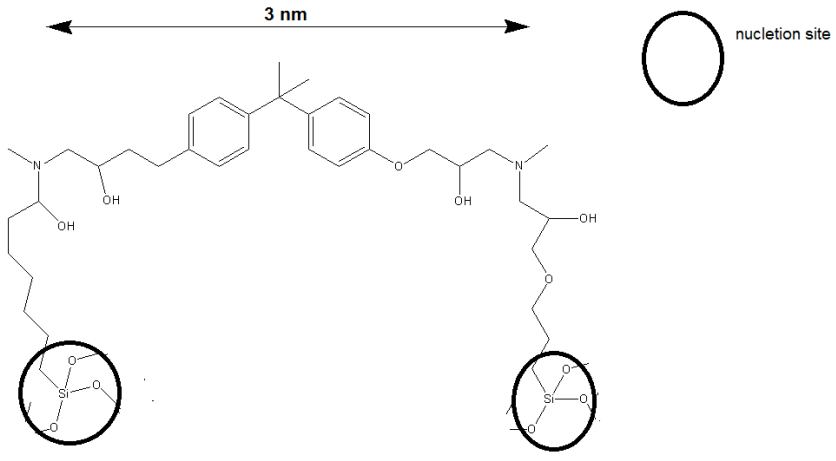

Fig. 20. Representation of two neighboring nucleation sites.

4.1.6 Polycondensation degree and local structure of silica

The local structure of the inorganic network is defined according to the number of oxygen bridging silicon atoms bonded to one (central) silicon atom. Common notations are Q^j for orthosilicates and T^j for organically modified silicates, where j is the number of siloxanes bridges attached to the silicon atom. Thus, Q^0 or T^0 denotes a silicon that does not have any O-Si bond attached, whereas Q^4 ot T^3 denotes a silicon that is fully connected to another silicon by an oxygen bridge.

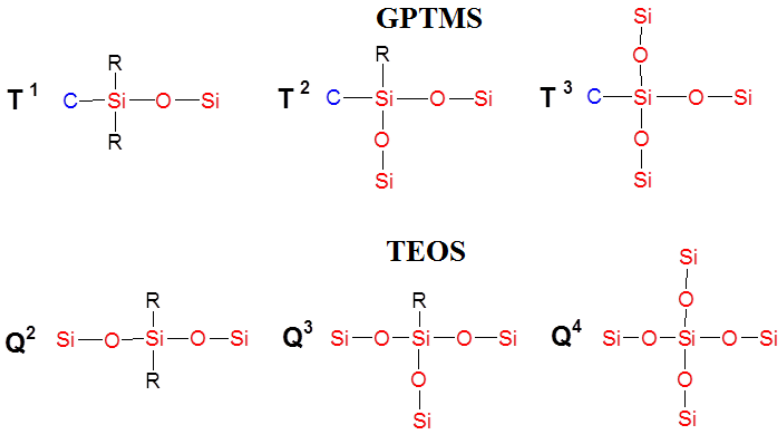

Fig. 21. Generic representation of the structures for the different T^J and Q^J groups. R=OH, OCH_3 (GPTMS) or OCH_2CH_3 (TEOS).

Although it is in principle possible to assign the different Q structures present in the inorganic network using Raman [21], the bands corresponding to Q^0 (673 and 730 cm^{-1}), Q^1 (608 and 596 cm^{-1}), Q^2 (525 cm^{-1}) and Q^4 (432 cm^{-1}) could not be assigned, owing to the fact that Raman signal for this epoxy-silica hybrid has a higher sensitivity for the Q^3 connectivity [22]. The proportions of T^j and Q^j species present in the G_0.5 and G_1 samples were extracted from the ^{29}Si NMR spectra by a peak fitting procedure used to determine the relative peak area for each local environment of Si. It is clear from Fig. 22 that the Q^4 and T^3 peaks (-107 ppm and -62 ppm respectively) have highest intensities in relation to the other peaks related to lower network connectivity, indicating the predominance in the inorganic network of a tetra- substituted TEOS and a tri-substituted GPTMS.

The degree of connectivity of the inorganic phase, known as the degree of poly-condensation (C_d), was determined for the G_0.5 and G_1 using following expression:

$$C_d = ((T^1 + 2T^2 + 3T^3) / 3 + (Q^1 + 2Q^2 + 3Q^3 + 4Q^4) / 4) * 100 \qquad \text{Eq. 12}$$

Where T^j and Q^j are the relative peak areas for the different local structures.
The determined C_d values for G_0.5, G_1/T_1 and G_1.5, T_1.5 ,T_2 are 87.8±2%, 85.8±2%, 94.7±2%, 87.1±2% and 87.8±2%, respectively (Table 6) which means that more than 83% of the silicon atoms are connected to another silicon atom through a siloxane bridge (Si-O-Si). The C_d values for the T series, prepared at higher TEOS addition, have value of 87%, whereas for the G series a extremely high connectivity of about 95% was determined. It seems that an increase of GPTMS favors the Q^4 structure; this perhaps explains why the signal-to-noise ratio for the Si-O-Si signal (485 cm^{-1}) in the Raman spectra decreases. In fact, this signal corresponds to the Q^3 structure and since the Q^4 configuration is favored, its signal intensity appears weaker as GPTMS is added. Although this result seems to be in contradiction with the hypothesis made above, that the extent of the organic network hinders the formation of the inorganic network, in fact increasing GPTMS concentrations leads to more compact silicon clusters (higher C_d values).

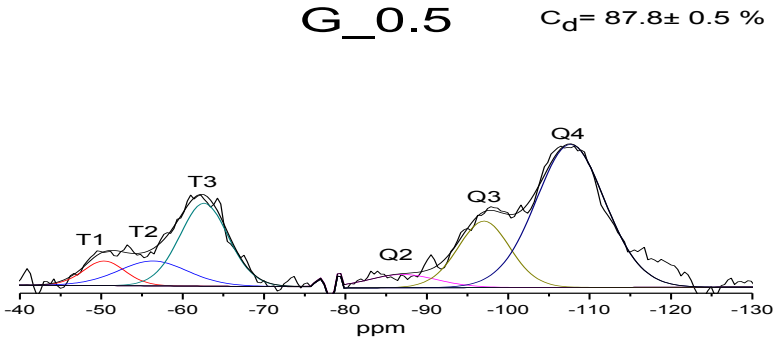

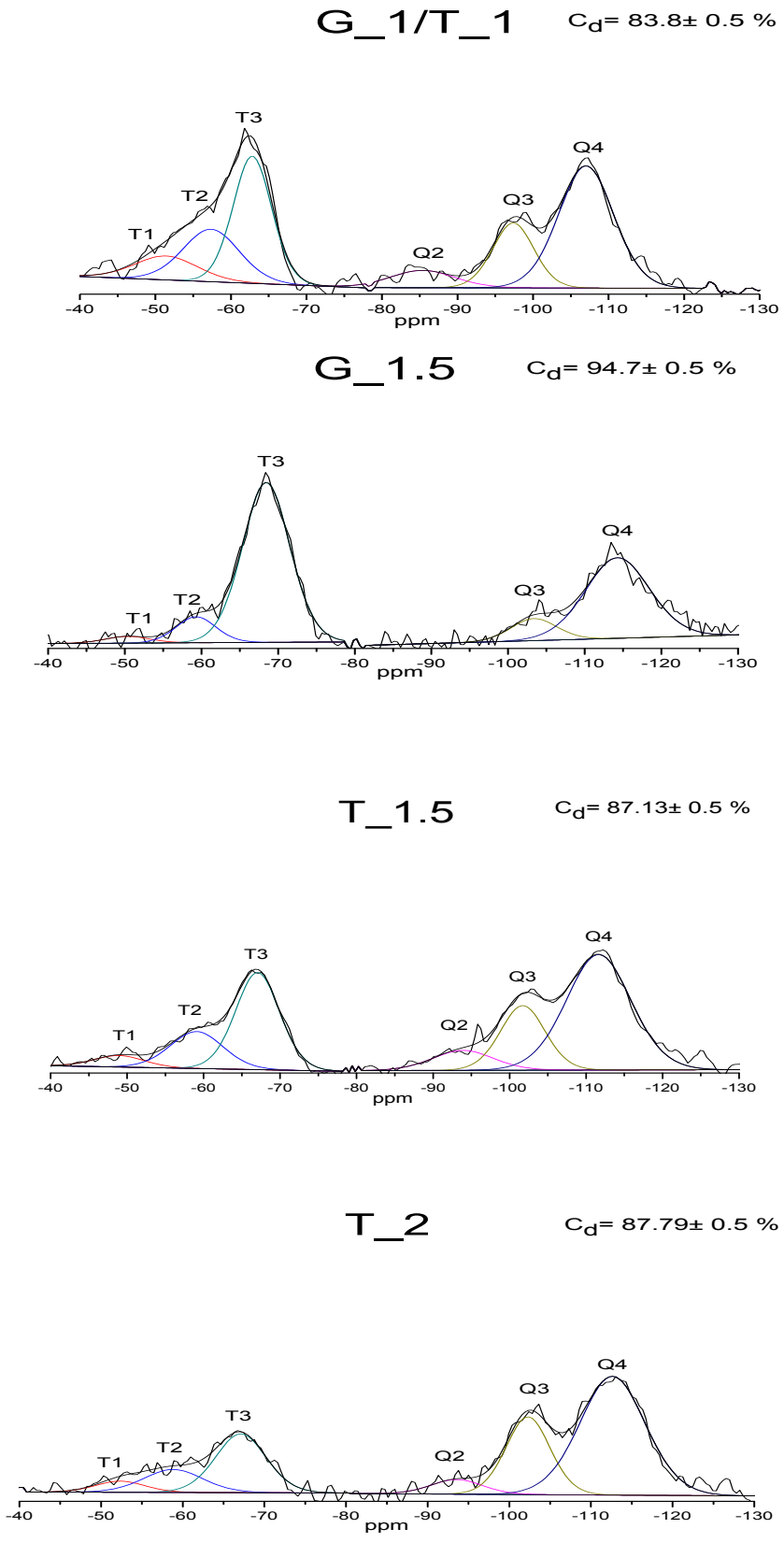

Fig. 22 . ^{29}Si NMR spectra for the different samples

Table 6. C_d values for the different sample

	G_0.5	G_1/T_1	G_1.5	T_1.5	T_2
C_d*%	87.8	85	94.7	87.1	87.8

*Experimental error ±2

Although ^{29}Si NMR has not been carried out for all the samples, the deconvoluted C 1s XPS spectra indicate by the correct relative intensity proportion of carbon species (Table 5), related to the polymeric phase, a complete hydrolysis of the alcoxy groups of GPTMS and TEOS. This leads to a highly polycondensed inorganic phase (Table 5), with elevated C_d values.

Table 7. Comparison of relative areas of the XPS C 1s spectral components with calculated nominal percentages for the different components.

	G_2 XPS	Completely hydrolyzed	Non hydrolyzed	G_2.5 XPS	Completely hydrolyzed	Non hydrolyzed
			(%)			
C-C	47.9	49.13	37.44	44.9	46.0	36.0
C-N	17.2	16.18	14.1	15.8	19.0	14.5
C-O	35.0	34.68	48.45	39.1	35.0	49.5

	T_2 XPS	Completely hydrolyzed	Non hydrolyzed	T_2.5 XPS	Completely hydrolyzed	Non hydrolyzed
			(%)			
C-C	48.22	52.44	37.87	48.7	52	36.05
C-N	14.77	16.0	11.61	14.7	16.0	11.05
C-O	36.46	31.46	50.5	34.8	31.46	52.88

4.2 Thermal analysis

4.2.1 Thermal analysis in a non-oxidative environment

The thermal properties of the hybrids were studied by thermogravimetry under nitrogen flow. DTG curves (Fig. 23) show that in a non-oxidative environment the cured epoxy-resins show a degradation process that involves 4 events: The first event (T1) above 200 °C is related to the elimination of the hydroxyl group (dehydration) [23] which leads to the formation of an unsaturated structure (Fig. 15). The principal event (T2) at 380 °C involves the scission of the allylic C-C bond (a) and allylic ether C-O bond [23,24], and the third event (T3) at about 440 °C is related to the breaking of N-C bonds [23]. The last event (T4) at around 530 °C is related to formation of siloxane bonds from partially condensed silanol ($SiO_x(OH)_y$) species [25]. The higher stability of the N-C bond with respect to the C-C bond is explained by the higher electronegativity of the nitrogen atom [26]. The dehydration reaction (Fig.24) favors a more stable structure due to the delocalization of the double C=C bonds into the aromatic ring's vicinity. Table 4 summarizes the main events during the decomposition of the hybrid.

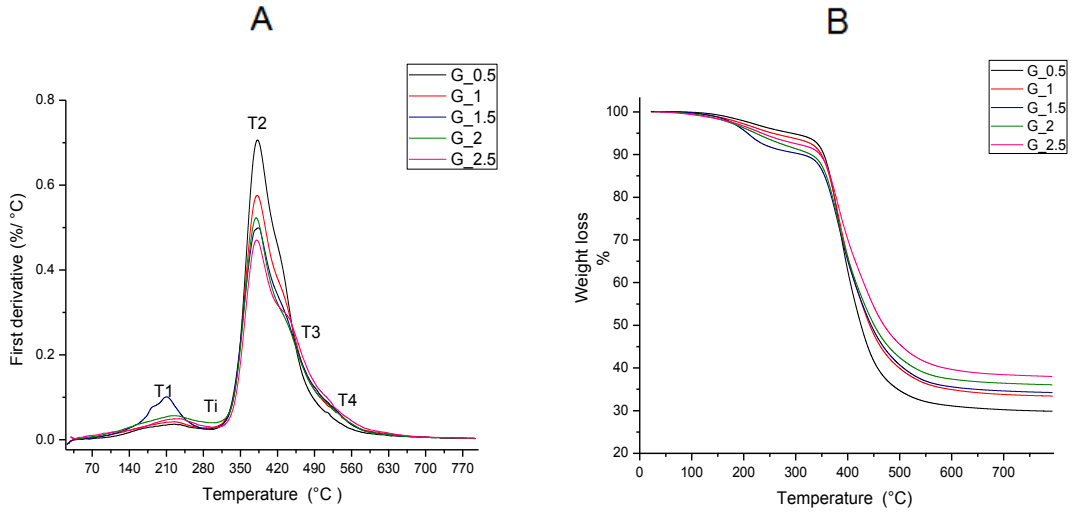

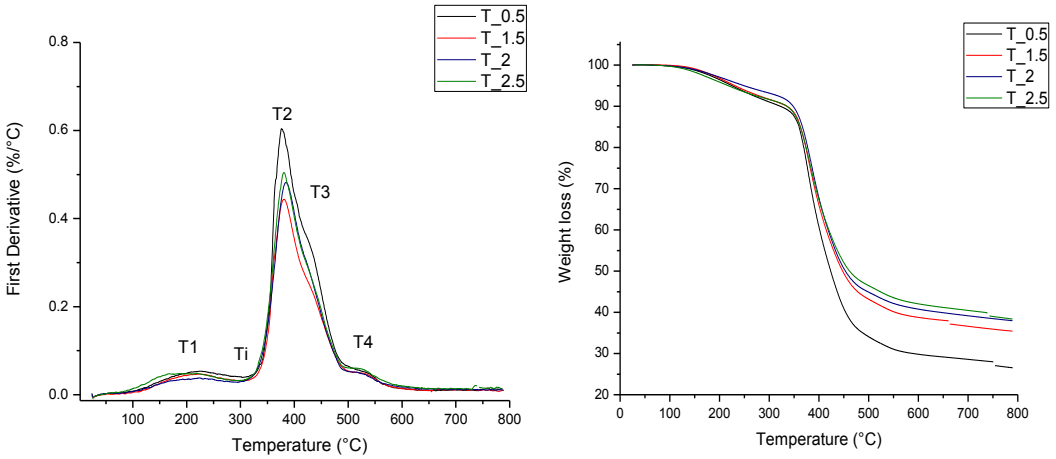

Fig 23. A) TG and B) DTG curves obtained for all hybrid samples.

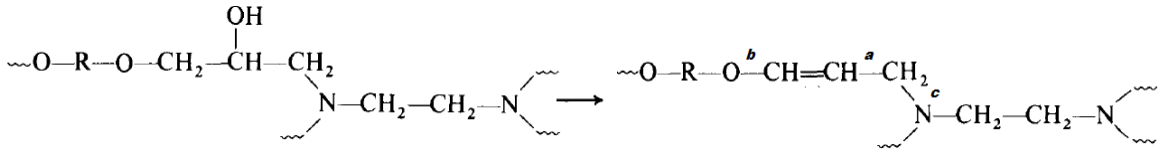

Fig 24. Dehydration process for cured epoxy resins, leading to the formation of an unsaturated structure.

Table 8. Main thermal decomposition events obtained for all hybrid samples

Sample	T_i (°C) Thermal stability	T1 (°C)	T2 (°C)	T3 (°C)	Si (at.%)	Residue (%)
G_0.5	285	382	435	528	4.8	30.0
G_1 (T_1)	293	382	441	528	5.2	33.5
G_1.5	297	382	435	528	5.6	34.2
G_2	304	384	451	528	6.0	36.0
G_2.5	306	382	451	528	6.3	38.0
T_0.5	306	377	440	538	4.4	26.6
T_1.5	314	380	442	540	5.9	35.6
T_2	295	385	430	535	6.8	37.0
T_2.5	302	380	430	533	7.5	38.4

As the first event (T1) is related to the dehydration, the critical temperature for the thermal stability, T_i, of the hybrid can be defined as the onset of the second event (Fig. 19). T_i is defined as temperature for 5% weight loss. It can be observed that the residue as well as the thermal stability increases as the content of siloxane content increases. However, no correlation was observed between the temperature of the main event of degradation (T2) and the silicon content. Dyakonov et al. [27] have shown that the main event in epoxy cured resins shifts towards higher temperatures when the cross-linking density increases. As the cross-linking density was kept constant for all hybrids (constant ratio of one epoxy to one N-H bond) the T2 event has an almost constant value of 540±10 °C for all samples. Above 750 °C the residue is still higher (35 - 40%) than expected for a low silicon content (4.4 - 7.5 at.%) of the hybrids. The FT-IR spectra of the residual material showed the presence of aliphatic (3000 - 2900 cm^{-1}) and aromatic carbon species (1580 cm^{-1}) and, as expected a strong peak at 1050 cm^{-1} corresponding to Si-O-Si bonds. This result indicates that the residue is composed of residual aliphatic and aromatic carbon and highly reticulated silica. The presented results show threshold temperatures Ti, marking the thermal stability at about 100 °C higher than that obtained for silica-PMMA films [28], showing the superior thermal properties of this material.

4.2.2 Thermal analysis in oxidative environment

DTG curve of the G_1/T_1 sample in an oxidative condition, show a degradation process that involves 2 events (Fig. 25): the first at 415 °C corresponds to the oxidation of the hybrid by a radical chain oxidation [1624], leading to the formation of amide groups. The second event at about 607 °C is associated to the random scission of the organic network [24]. In an oxidative environment the hybrid is thermally less stable than in a non-oxidative environment with T_i of about 170 °C. The residue determined at 800 °C for the G_1 sample in the oxidative environment is with 18.5 % (under nitrogen: 33.5 %) in agreement with its silicon content (5.2 at.%), confirming that under oxygen the residue is formed by pure silica.

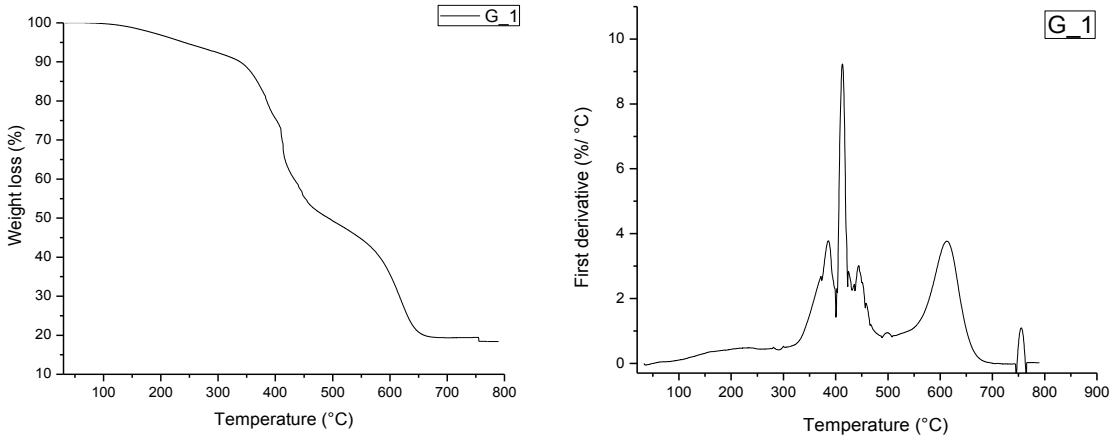

Fig 25. TG and DTG for G_1 under an oxidative environment. (Note that the small and narrow peaks in DTG a due to noise and consequently do not represent any characteristic event.)

4.3 Contact angle measurements

Contact angle measurements were performed using the static sessile drop method, to study the influence of increasing amounts of silica on the hydrophobicity of the hybrid surface. As the contact angle increases, the wettability of the material decreases, for $\Theta = 0°$ the liquid wets completely the surface, whereas for $\Theta = 180°$ the surface is super hydrophobic, and the liquid does not wet the surface. Generally when the contact angle of water is inferior to 90° the surface is known as hydrophilic, while when the contact angle is superior to 90° the surface is known as hydrophobic. All films deposited on carbon steel showed a contact angle that is inferior to 90° (Table 7), therefore they are slightly hydrophilic. However all the hybrids are more hydrophobic than carbon steel since its contact angle with water is 71.8°, whereas the contact angle with water of all hybrids is superior to 75°. Table 9 shows that for the G series the hydrophobicity of the films increases as the amount of silicon increases, however this is not observed for the T series, where the contact angle remains almost constant, at about 79°. It is known [29] that the use of organically modified silicates like GPTMS has the effect of lowering the surface tension thus increasing the contact angle of the material; this perhaps explains the difference observed between the G and T series.

Table 9. Contact angle as a function of silicon nominal percentage

Sample	Si (%)	Contact angle
G_0.5	4.8	75.69±0.20
G_1	5.2	77.78±0.41
G_1.5	5.6	76.78±0.14
G_2	6	83.43±0.43
G_2.5	6.3	86.75±0.49
T_0	3.2	79.40±0.22
T_0.5	4.4	79.17±0.47
T_1.5	5.9	62.68±0.39
T_2	6.8	79.10±0.32
T_2.5	7.5	79.69±0.60

The surface tension of the material is the sum of two contributions: the dispersive, that corresponds to van der Waal type-interactions, and polar related to hydrogen bonding type interactions. The dispersive and polar component of the hybrid's surface tension can be determined using the following equation [13,14]:

$$\cos(\Theta_m) = 2\ (\sigma_{sv}^d)^{0.5} * (\sigma_{lv}^d)^{0.5} / \sigma_{lv} + 2\ (\sigma_{sv}^p)^{0.5} * (\sigma_{lv}^p)^{0.5} / \sigma_{lv} - 1 \qquad \text{Eq. 13}$$

Where σ_{sv}^d and σ_{lv}^d are the dispersive and σ_{sv}^p and σ_{lv}^p are the polar components of the hybrid and liquid surface tensions. As hydroxyl and amine groups, responsible for the polar interactions (mainly in the form of hydrogen bonds), present only a very small part of the material, a good approximation is to ignore the polar composition and approximate Eq. 13 to a linear equation:

$$\cos(\Theta) = 2\ (\sigma_{sv}^d)^{0.5} * (\sigma_{lv}^d)^{0.5} / \sigma_{lv} - 1 \qquad \text{Eq. 14}$$

By determining the contact angle for different liquids, water, glycol and glycerin, it was possible to plot the data according to Eq. 14 and determine the intersect with the y axis. If the intersect is negative then dispersive forces dominate, resulting in poor adhesion. In contrast if the intercept is above the origin it is indicative of the action of polar forces across the interface, in addition to dispersion forces, hence improved wettability and adhesion is promoted [30,31]. Figures 26 and 27 display the resulting plots and Table.10 shows the intercept values for all hybrid samples. Although some differences were found between the hybrids, it is not possible to correlate the data with increasing amounts of silicon. However all samples of the G-series show negative intercepts, indicating that the dispersive component dominates, explaining their hydrophobic character (contact angles near 90°). Nonetheless none of the intercepts have values that are close to -1, showing that the polar components, even if weak, still exert some influence. For the T-series all intercept values are above 0, indicating a slightly hydrophilic character. It is important to note that all samples of the T-series have intercepts between 0.05 and 0.12 (except for T_1.5) reflecting that the addition of TEOS does not have a major influence onto the material's surface energy, explaining why the contact angle with water remains constant at around 79^{o} .

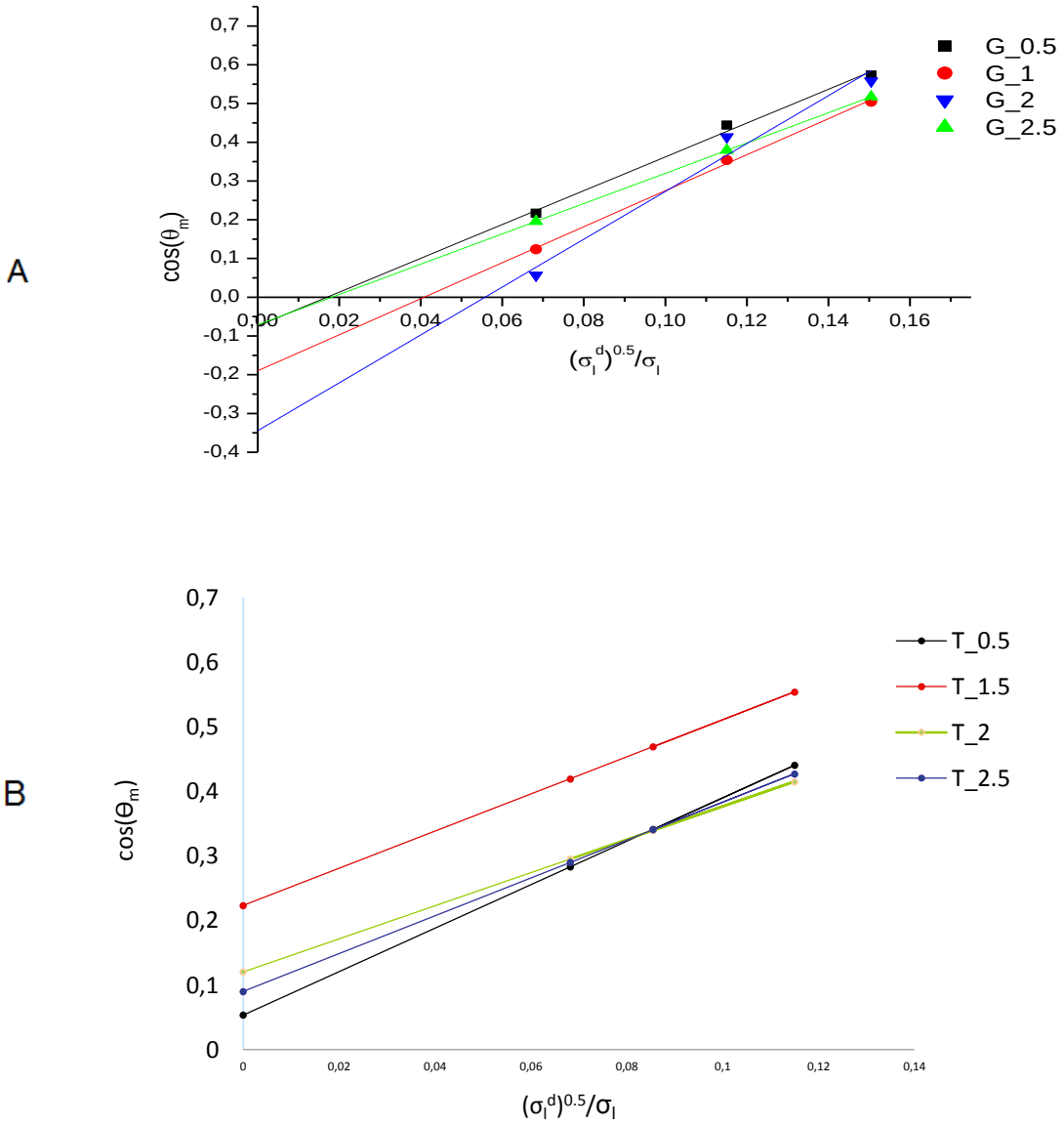

Fig. 26 $\cos(\Theta_m)$ as a function of $(\sigma_{lv}^d)^{0.5} / \sigma_{lv}$ for the G series (A) and for the T series (B).

Table 10. Shows the intercept with the y axis of the different

Samples	Intercept
G_0.5	-0.07
G_1	-0.19
G_2	-0.07
G_2.5	-0.34
T_0.5	0.05
T_1.5	0.22
T_2	0.12
T_2.5	0.09

4.4 Electrochemical Impedance

The anticorrosive performance of the hybrids were assessed by EIS, in a 3.5% NaCl saline solution at 25 °C. The hybrid films were deposited on carbon steel and attached to an electrochemical cell, then impedance measurements were performed as a function of time until a significative drop of the impedance modulus was observed, indicating the formation of a localized corrosion, known as pitting. The measurements were carried out in intervals of two days, and the day corresponding to the last measurement before the drop of the impedance has occurred was defined as the life span of the material. The principle of this technique consist in applying a sinusoidal potential, and to obtain, from the alternating current, the impedance of the electrochemical interface. The impedance Z(ω), has a real and imaginary part. That can be represented by a vector with modulus |Z|, where $|Z| = (Z^2_{real} + Z^2_{img})^{1/2}$. The angle between the vector |Z| and the x-axis is known as the phase angle ϕ. For every measurement, a Niquist plot, representing the real and imaginary part of the impendence, and Bode plots of the modulus of the impedance vs. the log of the frequency, ω, and a plot representing the phase angle as a function of the frequency were recorded. The modulus of the impendence at low frequencies is generally an indicator of the anticorrosive performance of the system. For example hybrid coatings having an initial modulus impedance of 10^8 Ωcm^{-2} typically show an excellent protection, whereas those below 10^6 Ω cm^{-2} offer a poor protection to the metallic substrate. The corrosion resistance of the films generally decreases with time. This decrease is generally associated with the

penetration of different ions species (principally Cl^-) by water uptake of the film, leading to an electrochemical reaction (corrosion) on the film/metal interface [32].

Figure 27 shows that for all the samples the phase angle graph possesses a large band that is composed at least of two time constants, one in the high frequencies (~10^4 Hz) and the other in the low frequencies (~ 2 Hz), related to coating regions of the film/electrolyte and the film/substrate interface, respectively. The phase angle has at high frequencies values above -80°, indicating a capacitive behavior for G_0.5 and T_1.5 over four decades and for T_2.5 for less than one decade. The latter result indicates a higher permeability of the T_1.5 hybrid structure. All the samples have modulus of impedance that are between 10^5 Ω cm^{-2} and 10^9 Ω cm^{-2}, the majority presenting a poor to medium corrosion protection efficiency. The samples containing intermediate GPTMS/TEOS and TEOS/GPMTS ratios, G_0.5 and T_1.5 present the highest modulus of impedance of 2 x 10^8 and 9 x 10^8 Ω cm^{-2}, respectively, and show a life span of several weeks. In contrast, for the G-series the samples prepared with the highest GPTMS to TEOS ratio have the lowest modulus of impedance (10^5 Ω cm^{-2} for G_2.5) with a life span of only 2 days. This behavior was not expected since the contact angle measurements showed for G_2.5 a higher hydrophobicity than that of G_0.5, indicating that mainly different structural characteristics might be responsible for the poor performance of the G_2.5 sample. For the T-series no correlation was observed between the ratio of TEOS and GPTMS and the modulus of impedance, however other "test" series (annexed data sheet) showed that the TEOS to GPTMS ratio between 1 to 1.5 (5 - 6 at.% of Si) always yields the best anticorrosive properties with modulus of impendence up to 4 x 10^9 Ω cm^{-2}.

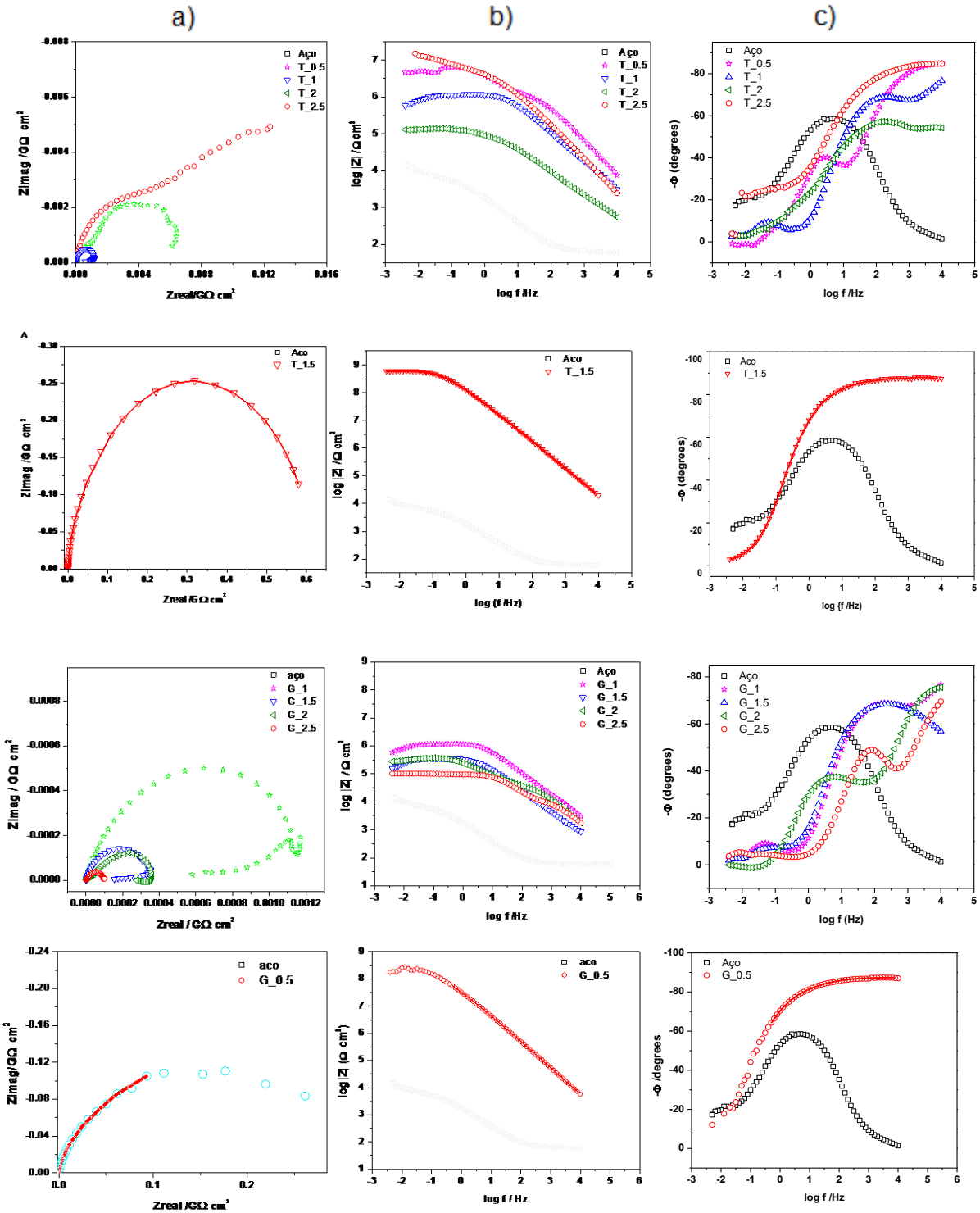

Fig. 27 Complex plane impedance Nyquist plot (a), and Bode plots ot the impedance modulus (b), and phase angle (c) plots vs. frequency of the hybrid samples after 1 day exposure in naturally aerated 3.5 % NaCl. Note that the T_1.5 and G_0.5 samples were fitted.

Table 11. Life span for the different hybrid films

Sample	Life span (days)
G_0.5	50
G_1	5
G_2	1
G_2.5	1
T_0.5	2
T_1.5	160*
T_2	1
T_2.5	4

*Still under measurement

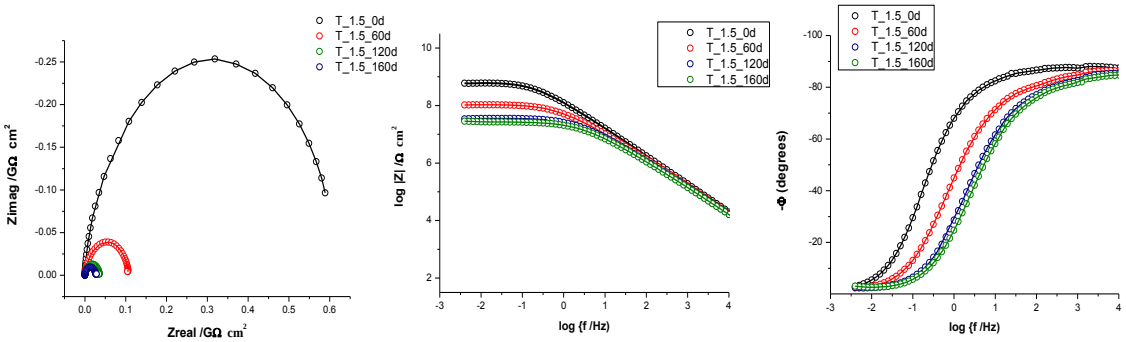

Fig 28. Complex plane impedance Nyquist plot (a), and Bode plots of the impedance modulus (b), and phase angle (c) plots vs. frequency of the T_1.5 hybrid for different times of immersion. Note that all the curves were fitted using the equivalent circuit in Fig 30.

Figure 28 shows Nyquist and Bode plots of the T_1.5 sample as a function of immersion time in 3.5% NaCl solution. It is observed that the impedance modulus drops from $10^9\ \Omega\ cm^2$ to only 10^7 after 160 days of immersion, indicating an excellent anticorrosive performance of this coating. The phase angle plot shows that after 160 days of immersion the ideal capacitive

behavior of the hybrid film drops from four to two decades, however, no pitting was detected.

The results indicate the existence of an optimum TEOS to GPTMS ratio which yields coatings with excellent anticorrosive properties which are similar to PMMA hybrid systems. [33] [34]

This is the result of a highly reticulated film, shown by an epoxy conversion and polycondensation degree (C_d) of almost 90 %, combined by an homogeneous hybrid network, as shown by SEM and SAXS, containing an inorganic phase which ensures a good adhesion of the film to the substrate. These promising results were obtained despite the mild conditions employed in the synthesis process: the inorganic network was prepared at room temperature and curing treatment did not exceed 60 °C .

Finally the EIS spectra for the samples showing the highest modulus of impedance (T_1.5 and G_0.5) after one day of immersion were adjusted using the following circuit

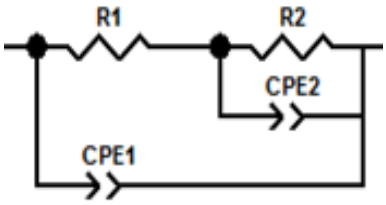

Fig. 29 Equivalent circuit used to fit EIS curves for samples with best anticorrosive performance.

The circuit has two time constants (CPE_1/R_1 and CPE_2/R_2). Where R_1 and R_2 are the film resistance and the charge transfer resistance, whereas CPE_1 and CPE_2 are the constant phase elements of the film and the capacitance due to the electrical double layer formed at the interface of the steel substrate. The impedance for circuit (Fig. 29) is given by the following expression [35]:

$$Z_A = (1/Z_1 + 1/(Z_2 + Z_{3,4}))^{-1} \quad \text{Eq. 15}$$

$$Z_A = jwC_1 + 1/(R_1 + R_2/(1+jwR_2C_2))^{-1} \quad \text{Eq. 16}$$

The real elements corresponding to the capacitors do not behave ideally, in this case the elements are represented by continues phase element (CPE), the relation between impedance and the frequency of CPE is given as follows :

$$Z_1 = 1/(jw)^n C \qquad \text{Eq. 17}$$

The admittance (Y) is equal to the inverse of the impedance, $Y = (jw)^n C$, a value of n =1 indicates and ideal capacitor, whereas a value of n=0.5 means that there is diffusion of the electrolytes into the film [36]

The capacitance of the film depends on the vacuum permittivity, ε_0, the dielectric constant of the material ε , the area of the material (A) and the thickness of the film (d):

$$C = \varepsilon_0 \varepsilon A/d \qquad \text{Eq. 18}$$

The dielectric constant of water is around 80.1 whereas the dielectric constant of organic films is typically around 4 to 8. Therefore water penetration results in the increase of the film´s capacitance. Overall a film having a capacitance value at around 10^{-9} F/cm^{-2} is indicative of good barrier properties [37]. In the case of a very low overpotential and when the system is in equilibrium the resistance of the film can be calculated using the following expression:

$$R_{ct} = RT/(n F i) \qquad \text{Eq. 19}$$

Where R is the ideal gas constant, T the temperature and n the electron density, F is the Faraday constant and i is the current density. If the coating remains intact, the current (i) remains low and the resistance high, however if corrosion is taking place the current (i) starts to increase and the value of resistance drops considerably. The results are shown in Figure 27 and Table 12 for G-0.5 and T_1.5

Table 12 Parameters obtained from the equivalent circuit for the G_0.5 and T_1.5 samples after one day of immersion.

	G_0.5_1d		T_1.5_1d	
χ^2	$6.83\ 10^{-5}$		$1.4\ 10^{-3}$	
R_{film} (Ω cm^2)	$8.6\ 10^{6}$	(20)	$5.3\ 10^{7}$	(19)
CPE_{film} (F cm^{-2} s^{-n})	$3.79\ 10^{-9}$	(0.7)	$1.1*10^{-9}$	(0.8)
n_{film}	0.97	(0.1)	0.97	(0.1)
R_{ct} (Ω cm^2)	$3.44\ 10^{8}$	(7.5)	$4.1\ 10^{8}$	(7.6)
CPE_{dl} (F cm^{-2} s^{-n})	$3.772\ 10^{-9}$	(3.0)	$1.25\ 10^{-9}$	(4.6)
n_{dl}	0.53	(2.6)	0.55	(5.4)

*values in parenthesis represent percentage errors

Both fits show a χ^2 value lower than 10^{-3}. Overall, both samples behave similar to ideal capacitors after one day of immersion, with n values close to 1. The capacitance for both films remains very low (10^{-9} F cm^{-2}) and the corrosion resistances are high (>10^6), showing a very low penetration of water and low current density, demonstrating that both films act as a very effective barrier against the diffusion of corrosive species.

The high value from the resistance of the electrical double layer (R_{ct}) comes from the fact that the contact surface area of the electrolytes with the substrate is very small (due to the very low porosity of the film) creating very high resistance values. [38][39]

Since water acts as a oxidative agent in the corrosion reaction resulting in the formation of rust, it is important to determine the water uptake which is given by the Brasher and Kingsbury's (BK) equation [40]:

$$\text{Water uptake } \% = \log(C_t/C_0) / \log_{(\varepsilon_{H20})} *100 \qquad \text{Eq. 23}$$

Where C_t is capacitance of the film at time t and C_0 is the capacitance of the film before the immersion, ε_{H20} is the dialectric constant of water (ε_{H20}= 78.3).

The determination of the effective capacitance at different times was determined using the following expression :

$$C_{eff} = Q^{1/n} R^{(1-n)/n} \qquad \text{Eq.24}$$

Where Q and n are the CPE parameters, and R the coating resistance. Fitting of the EIS data for T_1.5 sample at different times of immersion were performed by using the equivalent circuit below:

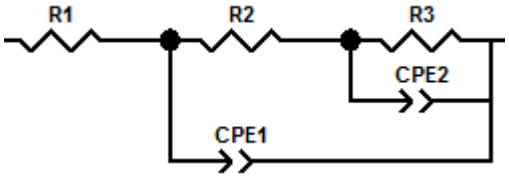

Fig. 30 Equivalent circuit used to fit the time dependence of the EIS curves.

In this case the resistance, R1, was added to the circuit, to take into account that after several days of immersion the resistance coming from the solution starts to have an effect in the impedance of the circuit. The results are shown in Figure 28 and Table 13, including water uptake values.

Table 13. Parameters obtained from the equivalent circuit for the T_1.5 for different times of immersion

	T_1.5_0d		T_1.5_60d		T_1.5_90d		T_1.5_160d	
χ^2	$2.1 *10^{-3}$		$8.7*10^{-5}$		$9.59*10^{-5}$		$1.1*10^{-3}$	
R_{film} (Ω cm^2)	$7.1*10^{7}$	(22)	$2.73*10^{6}$	(25)	$1.67*10^{6}$	(12)	$6.1*10^{5}$	(29)
CPE_{film} (F cm^{-2} s^{-n})	$1.0*10^{-9}$	(0.8)	$1.31*10^{-9}$	(3)	$1.51*10^{-9}$	(1)	$1.56*10^{-9}$	(1.6)
C_{eff}	$9.2*10^{-10}$		$1*10^{-9}$		$1.1*10^{-9}$		$1.1*10^{-9}$	
n_{film}	0.97	(0.1)	0.96	(0.3)	0.95	(0.1)	0.95	(0.1)
R_{ct} (Ω cm^2)	$6*10^{8}$	(8)	$1.1*10^{8}$	(1.5)	$2.1*10^{7}$	(16)	$2.3*10^{7}$	(19)
CPE_{dl} (F cm^{-2} s^{-n})	$8.6*10^{-10}$	(5)	$2.8*10^{-9}$	(1.7)	$2.6\ 10^{-9}$	(23)	$4.9 *10^{-9}$	(19)
n_{dl}	0.57	(6)	0.58	(1.1)	0.67	(5.5)	0.58	(5)
R_{water}	0		0		18.79	(4.3)	15.74	(6.4)
Water Uptake	0		1.91 %		4.1 %		4.1%	

*values in parenthesis represent percentage errors

After 160 days of immersion the hybrid still behaves close to an ideal capacitor having an n value that is almost equal to unity (0.95). The water uptake increases with the time of immersion representing 10 % of the volume of the coating after 160 days of immersion. Two trends can be observed: the first is a rapid increase in the water uptake (from day 0 to 120), probably obeying the Fickian law of diffusion, and the second (from day 120 to 160) where the uptake shows a saturation behavior. The capacitance of the electrical double layer remains very low ($5\ 10^{-9}$ F cm^{-2}) and remains almost unchanged after 60 days of immersion. Because the capacitance of a Helmholtz double layer is around 10 to 40 μF cm^{-2}, we can infer that there is very low penetration of the electrolytes into the film and that no pitting corrosion has occurred. The capacitance values of the film, increases over time due to the penetration of water, however it remains stable at 10^{-9} F cm^{-2}, indicating that after 160 days the film still has good barrier properties.

5. CONCLUSIONS

Epoxy silica hybrids having a concentration of 5 to 6 % of Silicon always show the best anticorrosive performance, standing for more than 160 days in a saline solution. This is despite the mild conditions employed in the synthesis process, not only resulting in a highly reticulated hybrid but also in a material with enhanced thermal properties, having threshold temperatures (Ti) at about 100 °C higher than that obtained for silica-PMMA. The main conclusions from this work are listed below :

- AFM results shows defect free epoxy-silica hybrid films with low surface roughness, however the presence of localized elevations in the surface of the films are presently not clear.
- Quantitative XPS analysis shows good agreement with the nominal percentage calculated for each sample, indicating that no major losses of the precursors have occurred during the synthesis.
- Micro Raman of the surface of the film demonstrates the opening of the oxirane ring as well as the formation of the silicate network. Band integration of the epoxy band at 911 cm^{-1} in the FT-IR spectra indicates an epoxy conversion at around 85% for the T series.
- ^{29}Si NMR shows a highly condensed inorganic network with a polycondensation degree up to 95 %.
- The epoxy-silica hybrids are thermally stable up to ~300 °C, and suitable for applications in the intermediate temperature range. The degradation process of the hybrid under nitrogen flow involves only one main event at about 380 °C that corresponds to the scission of the allylic C-C bond. The high residue at 800 °C of 35% - 40% was identified as aliphatic and aromatic structures and Si-O-Si bonds from the inorganic network. Under oxygen the hybrid show two main events, the residue is lower that nitrogen, and is formed by pure silica.
- Contact angle measurements showed a hybrid surface that is more hydrophobic than carbon steel. Higher concentration of GPTMS increase the hydrophobic character of

the hybrid, whereas higher concentration of TEOS does not have any effect on the hydrophobicity of the material.

- The hybrid coatings have a medium to high corrosion protection efficiency, with modulus of impendence varying from 10^5 Ω cm^{-2} to 10^9 Ω cm^{-2}. The G_0.5 and T_1.5 samples have the highest modulus of impedance (2 x10^8 and 9 x 10^8 Ωcm^{-2}) being up to 23 weeks in a 3.5% saline solution.
- Additional "test-series" series have shown that samples with nominal concentrations of 5 to 6% of silicon tend to have the best anticorrosive properties.

6. PERSPECTIVES

- A new series, studying the influence of the temperature of deposition of the film could be made, in fact recent tests have shown that films deposited at high temperatures (around 70 ^{0}C) always have better anticorrosive properties.

- The thermal properties of the epoxy-silica hybrids could be further improved by choosing aromatic amine hardeners .

- New synthetic routes could be explored, in fact the time of the curing reaction of epoxy resins can be dramatically reduced by using microwave ovens or UV-light.

- Mechanical tests could be performed (scratching, wearing and hardness tests).

REFERENCES

1 KHRAMOV, A. N.; BALBYSHEV, V. N.; VOEVODIN, N. N.; DONLEY, M. S. Nanostructured sol-gel derived conversion coatings based on epoxy- and amino-silanes. **Progress in Organic Coatings**, v. 47, p. 207-213, Sept. 2003.

2 COLE, K. C.; HECHER, J. J.; NOEL, D. A new approach to modeling the cure kinetics of epoxy amine thermosetting resins 2. Application to a typical system based on bis 4-(diglycidylamino)phenyl methane and bis(2-aminophenyl) sulphone. **Macromolecules**, v. 24, n. 11, p. 3098-3110, May 1991.

3 SANCHEZ, C.; ROZES, L.; RIBOT, F.; LABERTY-ROBERT, C.; GROSSO, D.; SASSOYE, C.; BOISSIERE, C.; NICOLE, L. "Chimie douce": a land of opportunities for the designed construction of functional inorganic and hybrid organic-inorganic nanomaterials. **Comptes Rendus Chimie,** v. 13, n. 1/2, p. 3-39, Feb. 2010.

4 MOLINA, E. F.; MARCAL, L.; CARVALHO, H. W. P. D.; NASSAR, E. J.; CIUFFI, K. J. Tri-ureasil gel as a multifunctional organic-inorganic hybrid matrix. **Polymer Chemistry**, v. 4, n. 5, p. 1575-1582, 2013.

5 SARMENTO, V. H. V.; SCHIAVETTO, M. G.; HAMMER, P.; BENEDETTI, A. V.; FUGIVARA, C. S.; SUEGAMA, P. H.; PULCINELLI, S. H.; SANTILLI, C. V. Corrosion protection of stainless steel by polysiloxane hybrid coatings prepared using the sol-gel process. **Surface and Coatings Technology**, v. 204, n. 16/17, p. 2689-2701, 2010.

6 BRINKER, C. J.; SCHERER, G. W. Hydrolisis and condensation II: silicates. In: _____. **Sol-gel science**: the physics and chemistry of sol-gel processing. San Diego: Academic Press, 1990. Chap. 3, p. 99-108.

7 AIROLDI, C.; FARIAS, R. F. Alcóxidos como precursores na síntese de novos materiais através do processo sol-gel. **Química Nova**, v. 27, n. 1, p. 84-88, 2004.

8 BRUSCIOTTI, F.; SNIHIROVA, D. V.; XUE, H.; MONTEMOR, F. M.; LAMAKA, S. V.; FERREIRA, M. G. S. Hybrid epoxy–silane coatings for improved corrosion protection of Mg alloy. **Corrosion Science**, v. 67, p. 82-90, Feb. 2013.

9 NAM, Y.; BRANCH, D. W.; WHEELER, B. C. Epoxy-silane linking of biomolecules is simple and effective for patterning neuronal cultures. **Biosensors and Bioelectronics**, v. 22, p. 589-597, Dec. 2006.

10 GLATTER, O.; KRATKY, O. (Ed.). **Small-angle scattering of X-ray**. New York: Academic Press, 1982. 515 p.

11 BEAUCAGE, G. Approximations leading to a unified exponential power-law approach to small-angle scattering. **Journal of Applied Crystallography**, v. 28, p. 717-728, 1995.

12 BEAUCAGE, G.; ULIBARRI, T. A.; BLACK, E. P.; SCHAEFER, D. W. Multiple size scale structures in silica-siloxane composites studied by small-angle scattering. In: MARK, J. E.; LEE, C. Y.-C.; BIANCONI, P. A. (Ed.). **Hybrid organic-inorganic composites**. Washington, DC: American Chemical Society, 1995. Chap. 9, p. 97-111. (ACS symposium series, 585).

13 OWENS, D. K.; WEND, T. R. C. Estimation of the surface free energy of polymers. **Applied Polymer Science**, v. 13, p. 1741-1747, July 1969.

14 KAELBLE, D. H.; UY, K. C. A reinterpretation of organic liquid-polytetrafluoroethylene surface interactions. **The Journal of Adhesion**, v. 2, p. 50-60, 1970.

15 RAHAMAN, M. N. **Ceramic processing and sintering**. 2nd ed. Boca Raton: CRC Press, 2003. 875 p.

16 GONZÁLEZ, M.; CABANELAS, J. C.; BASELGA, J. Applications of FTIR on epoxy resins identification, monitoring the curing process, phase separation and water uptake. In: THEPHANIDES, T. **Infrared spectroscopy**: materials science, engineering and technology. Rijeka: InTech, 2012. Chap. 13, p. 261-284.

17 REN, M. **Comparison of near infrared and Raman spectroscopies for noninvasive clinical measurements**. 2007. 181 f. Thesis (Doctor of Philosophy) - University of Iowa, Iowa, 2007.

18 STEVEN, R.; DAVIS, S. R.; BROUGH, A. R.; ATKINSON, A. Formation of silica/epoxy hybrid network polymers. **Journal of Non-Crystalline Solids**, v. 315, p 197-205, June 2001.

19 DAHMOUCHE, K.; CARLOS, L. D.; ZEA BERMUDEZ, V.; SA FERREIRA, R. A. ; SANTILLI, C. V.; CRAIEVICH A. F. Structural modelling of Eu3z-based siloxane–poly(oxyethylene) nanohybrids. **Journal of Material Chemistry**, v. 11, p. 3249-3257, Sept. 2011.

20 ZAIONCZ, S.; DAHMOUCHE, K.; PARANHOS, C. M.; SAN GIL, R. A. S. ; SOARES, B. G. Relationships between nanostructure and dynamic-mechanical properties of epoxy network containing PMMA-modified silsesquioxane. **Express Polymer Letters**, v. 3, n. 6, p. 340-351, 2009.

21 LIPPERT, J. L.; MELPOLDER, S. B.; JOHNSON, A. F. FT-Raman spectroscopic monitoring of the group-transfer polymerization of methyl methacrylate. **Vibrational Spectroscopy**, v. 41, p. 160-169, 2006.

22 ZHANG, S. L. **Raman spectroscopy and its application in nanostructures**. 2nd ed. New York: Wiley, 2012. 500 p.

23 BELLENGER, V.; FONTAINE, E.; FLEISHMANN, A.; SAPORITO, J.; VERDU, J. Thermogravimetric study of amine cross-linked epoxies. **Polymer Degradation and Stability**, v. 9, p. 195-208, 1984.

24 PUGLIAA, D.; MANFREDIB, L. B.; VAZQUEZ, A.; KENNYA, J. M. Thermal degradation and fire resistance of epoxy–amine–phenolic blends. **Polymer Degradation and Stability**, v. 73, p. 521-527, 2001.

25 LANDRY, C. J. T.; COLTRAIN, B. K.; WESSON, J. A.; ZUMBULYADIS, N.; LIPPERT, J. L. In situ polymerization of tetraethoxysilane in polymers: chemical nature of the interactions. **Polymer**, v. 33, n. 7, p. 1496-1506, 1992.

26 GRASSIE, N.; GUY, M. I.; TENNENT, N. H. Degradation of epoxy polymers: part 4 thermal degradation of bisphenol-A diglycidyl ether cured with ethylene diamine. **Polymer Degradation and Stability**, v. 14, p. 125-137, 1986.

27 DYAKONO, T.; MANN, P. J.; CHEN, Y.; STEVENSON, W. T. K. Thermal-analysis of some aromatic amine cured model epoxy-resin. 2. Resisdues of degradation. **Polymer Degradation and Stability**, v. 54, p. 67-83, 1996.

28 WANG, Y. T.; CHANG, T. C.; HONG, Y. S.; CHEN, H. B. Effect of the interfacial strucuture on the thermal stability of poly(methyl methacrylate) –silica hybrids. **Thermochimica Acta**, v. 397, p. 219-226, 2003.

29 KULINICH, S. A.; FARZANEH, M. Alkylsilane self-assembled monolayers: modeling their wetting characteristics. **Applied Surface Science**, v. 230, p. 232-240, 2004.

30 FOWKES, F. M. Attractive forces at interfaces. **Industrial Engineering Chemistry**, v. 56, p. 40-52, 1964.

31 CHATTORAJ, D. K.; BIRDI, K. S. **Adsorption and the Gibbs surface excess**. New York: Plenum Press, 1984. 451 p.

32 McINTYRE, J. M.; PHAM, H. Q. Electrochemical impedance spectroscopy; a tool for organic coatings optimizations. **Progress in Organic Coatings**, v. 27, p. 201-207, 1996.

33 HAMMER, P.; SANTOS, F. C. dos; CERRUTTI, B. M.; PULCINELLI, S. H.; SANTILLI, C. V. Highly corrosion resistant siloxane-polymethyl methacrylate hybrid coatings. **Journal of Sol-Gel Science and Technology**, v.63, p. 266-274, 2012.

34 SARMENTO, V. H. V.; SCHIAVETTO M. G.; HAMMER, P. ; BENEDETTI, A. V.; FUGIVARA , C. S.; SUEGAMA, P. H.; PULCINELLI, S. H. ; SANTILLI, C. V. Corrosion protection of stainless steel by polysiloxane hybrid coatings prepared using the sol–gel process. **Surface and Coatings Technology**, v. 204, p. 2689-2701, May 2010.

35 ORAZEM, M. E.; TRIBOLLET B. **Electrochemical impedance spectroscopy**. New Jersey: Wiley, 2008. 523 p.

36 GAMRY INSTRUMENTS. **Basics of electrochemical impedance spectroscopy**. Warminster, 2014. 31 p.

37 LOVEDAY, Y. D.; PETERSON, P.; RODGERS, B. Evaluation of organic coatings with electrochemical impedance spectroscopy. Part 2: application of EIS to coatings. **Journal of Coating Technology**, v. 1, n. 10, p. 88-93, 2004.

38 YUAN, X.; YUE, Z. F.; CHEN, X.; WEN, S. F; LI, L.; FENG, T. EIS study of effective capacitance and water uptake behaviors of silicone-epoxy hybrid coatings on mild steel. **Progress in Organic Coatings**, v. 86, p. 41-48, Sept. 2015.

39 DUARTE, R. G. ; CASTELA, A. S. ; FERREIRA, M. G. S. A new model for estimation of water uptake of an organic coating by EIS: the tortuosity pore model. **Progress in Organic Coatings**, v. 65, n. 2, p. 197-205, June 2009.

40 BRASHER, D. M.; KINGSBURY, A. H. Electrical measurements in the study of immersed paint coatings on metal. I. Comparison between capacitance and gravimetric methods of estimating water-uptake. **Journal of Applied Chemistry**, v. 4, n. 2, p. 62-72, Feb. 1954.